applied sciences

MDPI

Review

Copper- and Iron-Based Nanoflowers in Cancer Theranostics

Agathi Vlachou, Despina A. Gkika, Pavlos Efthymiopoulos, George Z. Kyzas * and Alexandros Tsoupras *

Hephaestus Laboratory, School of Chemistry, Faculty of Sciences, Democritus University of Thrace, St Lukas, 65404 Kavala, Greece; agblach@chem.duth.gr (A.V.); degkika@chem.duth.gr (D.A.G.); pefthym@chem.duth.gr (P.E.)

* Correspondence: kyzas@chem.duth.gr (G.Z.K.); atsoupras@chem.duth.gr (A.T.)

Abstract: In recent years, nanoscience and nanotechnology have gained prominence within materials science, offering new opportunities for cancer diagnosis and treatment. Advances in nanotechnology have allowed for the manipulation and size control of nanomaterials, leading to the development of a wide range of materials. The use of nanomaterials as chemical biology tools in cancer theranostics has been widely investigated, owing to their enhanced stability, biocompatibility, and improved cell permeability. These properties enable precise targeting while addressing the limitations of conventional cancer treatments. Nanoflowers, a specific class of nanomaterials, have recently attracted significant interest due to their promising properties for several biomedical applications. However, despite the growing attention toward nanoflowers, detailed reviews on the subject have been limited. This work focuses on two primary types of hybrid nanoflowers: iron- and copper-based ones. Within this article an overview of recent applications in cancer theranostics are thoroughly reviewed, while the synthesis processes for controlling morphology and size, underlying functions, and their characteristics and uses are also extensively explored, aiming to provide a guide for future developments in the field.

Keywords: anticancer; antitumor; metal nanoparticles; metal oxide nanoparticles; nanostructured materials; hybrid nanomaterials

check for updates

Citation: Vlachou, A.; Gkika, D.A.; Efthymiopoulos, P.; Kyzas, G.Z.; Tsoupras, A. Copper- and Iron-Based Nanoflowers in Cancer Theranostics. *Appl. Sci.* **2024**, *14*, 11294. https://doi.org/10.3390/app142311294

Academic Editors: Francesca Brero and Manuel Mariani

Received: 3 November 2024
Revised: 20 November 2024
Accepted: 28 November 2024
Published: 4 December 2024

Copyright: © 2024 by the authors. Licensee MDPI, Basel, Switzerland. This article is an open access article distributed under the terms and conditions of the Creative Commons Attribution (CC BY) license (https://creativecommons.org/licenses/by/4.0/).

1. Introduction

Despite various advancements and the introduction of cutting-edge technologies in medical sciences, cancer remains a significant global public health concern [1]. It accounted for an estimated 9.6 million deaths in 2018. Projections suggest that cancer could soon surpass heart disease as the leading common cause of death [2]. Typical treatments are often less effective and can cause serious damage to healthy cells, worsening patients' condition [3,4]. Consequently, there is a constant global demand for more effective cancer treatments [4].

In this regard, the rise of nanotechnology offers new avenues for early cancer diagnosis and treatment. Nanotechnology, particularly through the modification of various nanoparticles (NPs), has been extensively utilized in biomedical research [5]. NPs offer several unique advantages: their small size allows for easy metabolism by the body, and their large surface area enables them to carry therapeutic drugs, prolong drug action, enhance efficacy at lower doses, and reduce side effects [6–10]. Nano-PROTAC offers solutions to challenges such as poor water solubility, limited cell permeability, off-target effects, and metabolic instability [11]. Tao et al., introduced a nanoengineering approach (Nano-PROTACs) by encapsulating ARV-771 within glutathione (GSH)-responsive polydithiamide polymer (PDSA) nanoparticles, which enhanced BRD4 protein degradation and suppressed downstream oncogene c-Myc expression [12]. In another study, a homogeneous anti-MHC-II nanobody–drug conjugate (VHH7-DM1) was developed using Sortase A (SrtA)-mediated protein conjugation. This conjugate demonstrated efficacy in both in vitro and in vivo models for treating aggressive murine B-cell lymphoma. With superior pharmacokinetics, VHH conjugates surpassed commercial monoclonal antibodies (mAbs) in terms of internalization

and clearance, offering reduced systemic toxicity and enabling convenient non-invasive imaging [13].

As a result, NPs are considered powerful theranostic tools with multiple biomedical applications [14,15]. Theranostics is a cutting-edge strategy that integrates therapy and diagnosis into a single platform for accurate cancer detection. It is considered a promising advancement in addressing the challenges of conventional cancer treatments. Nanoparticles (NPs) are especially effective as carriers for theranostic agents due to their exceptional physicochemical properties [16].

Previous applications have imposed varied requirements on nanostructures, leading to the development of a wide array of nanoparticle types. Among these, metal nanoparticles, particularly copper [17,18] and iron [19,20], have become indispensable in biomedicine due to their tunable properties and biocompatibility [21,22], establishing them as a promising category. For instance, copper is present in many proteins and enzyme catalytic sites [23], and its oxides offer a multitude of advantages, such as inducing oxidative stress for tumor destruction and catalyzing oxygen production from endogenous hydrogen peroxide (H_2O_2) to alleviate tumor hypoxia [24]. Similarly, transition metals like iron (Fe) enhance the fundamental properties of nanomaterials, increasing their functionality and offering flexibility to meet the specific requirements of various applications [25]. The performance of metal oxides can be precisely adjusted by controlling factors like size, shape, composition, and structure, rather than relying solely on their chemical composition [26,27]. With this level of precision, the use of metal oxides reaches new heights, where their performance can be significantly impacted by slight manipulations, sometimes making it challenging to select the most suitable candidate for a given application.

In addition to other nanostructures, a new category of NPs owing structural parts smaller than 100 nm [28] known as nanoflowers (NFs), has recently captured extensive attention. Their structure enhances surface reactions, offering benefits such as strong adsorption capacity, great catalytic ability, and efficient drug loading potential [29]. NFs can be produced from a range of organic and inorganic materials, including polymers, metals, metal oxides, and carbon. Additionally, hybrid nanoflowers (HNFs) made from DNA, proteins, enzymes, and polymers are also a significant area of interest [30]. In 2012, Zare and his team created an organic–inorganic hybrid—by adding Cu(II) sulfate to phosphate-buffered saline containing a protein, expanding the focus beyond metal NFs [31]. This discovery paved the way for new nanohybrids, expanding the scope of nanoflower research. These NFs possess a distinctive geometry, with petal- or branch-like structures radiating from a central core, resembling natural flowers [32]. The unique design of NFs is achieved through controlled synthesis involving seed-mediated growth, optimized reactions, and selected precursor materials [33]. Their layered structure enhances adsorption capacity, electrocatalytic activity, loading capacity, and stability [34]. Hybrid nanoflowers composed of metal ions and polymers exhibit unique characteristics.

Recently, multiple reviews have explored the synthesis of nanoflowers. Yucheng Liu and his team offered an in-depth analysis of hybrid nanoflowers, covering their design, synthesis methods, mechanisms, and properties. They also emphasized advanced biomedical applications such as biosensing, biocatalysis, and cancer treatment [35]. In 2022, Su Jung Lee and team reviewed inorganic nanoflowers, emphasizing their applications in various treatments, including cancer therapy. Two years later, the same group released another review that categorized inorganic nanoflowers into categories according to their attributes. They discussed preparation methods, morphology, size control, mechanisms, and possible uses to advance future research and promote synergistic implementations across various fields [36]. Mehrdad Khakbiz and his team investigated the synthetic methods, properties, and biomedical applications of various nanostructures, including nanoflowers and other nanostructures. Their work provides insights into their use as advanced functional materials for a wide range of applications. Chormey et al., published a recent review that focuses on the synthesis, characterization, and analytical applications of nanoflowers.

The review covers a range of synthesis techniques, including sol–gel, hydrothermal and biosynthesis [33].

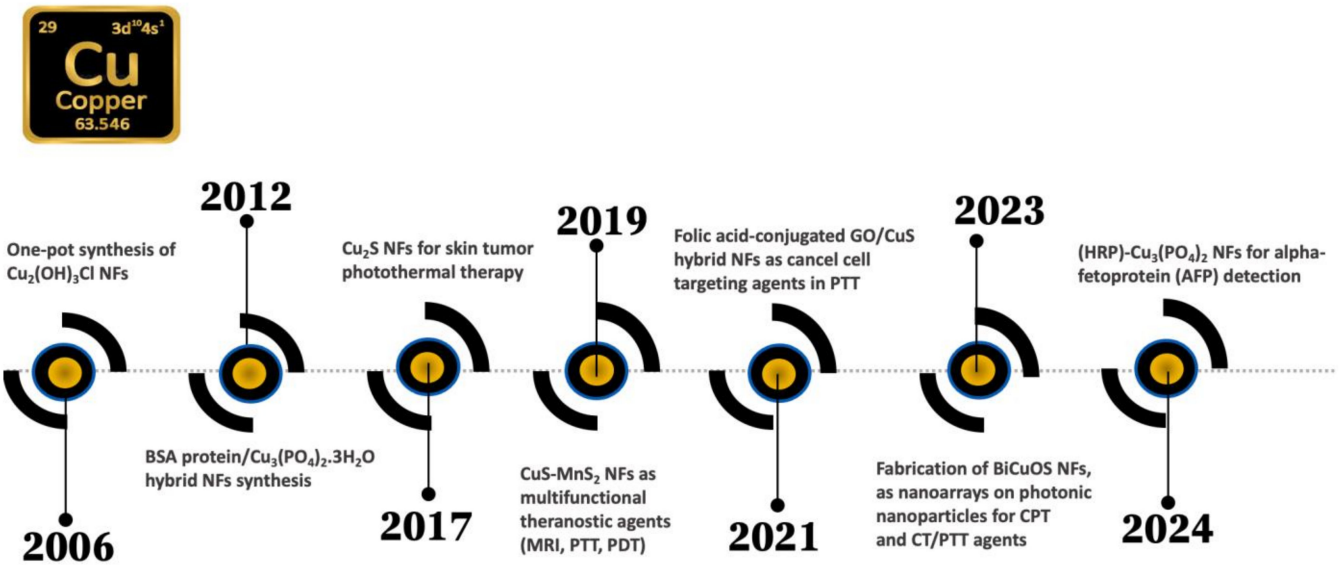
To date, nanoflowers with metal compositions present certain challenges, particularly in design strategies, as their performance can vary significantly depending on the approach used [35]. This complexity has led to inconsistent experimental results. For example, copper ions have been shown to negatively affect the enzyme β-galactosidase [37], while for other proteins like laccase, copper ions in the nanoflower structure can enhance the enzyme's activity, as seen in the case of $Cu_3(PO_4)_2$ NFs [31]. To address this issue, one potential solution is to develop new nanostructured materials that combine multiple metals and allow precise control over the metal ratio. Such a fine manipulation of metal oxides can significantly impact performance, making it challenging to select the ideal candidate for specific applications. However, the use of mixed-metal nanoparticles offers various benefits [38–40], such as improved attributes through synergistic effects, tailored functionalities, stability and cost efficiency.

Given the scarcity of comprehensive reviews on the applications of NFs, particularly those with metallic compositions, this review aims to outline the role of iron- and copper-based NFs in cancer theranostics. First, we elaborate on the mechanisms of various synthetic methods based on previously reported strategies. Then, we classify copper- and iron-containing hybrid nanoflowers, synthesized using different organic components and metal precursor salts, according to their specific applications in cancer diagnosis and therapy, providing valuable insights and guidance for future design.

Thus, this review serves two main purposes: firstly, to offer up-to-date perspectives on the use of copper and iron nanoflowers as tools in cancer theranostics; and secondly, to evaluate how the synthesis process impacts nanoflower performance. In essence, it captures significant progress made over the past five years in applying copper and iron nanoflowers for cancer treatment. A key focus is on the novel aspects of the synthesis process, assessing its influence on nanoflower performance. Additionally, we explore the mechanisms and strategies involved in synthesizing iron and copper nanoflowers and finish with a discussion on the prospects of this promising area of research.

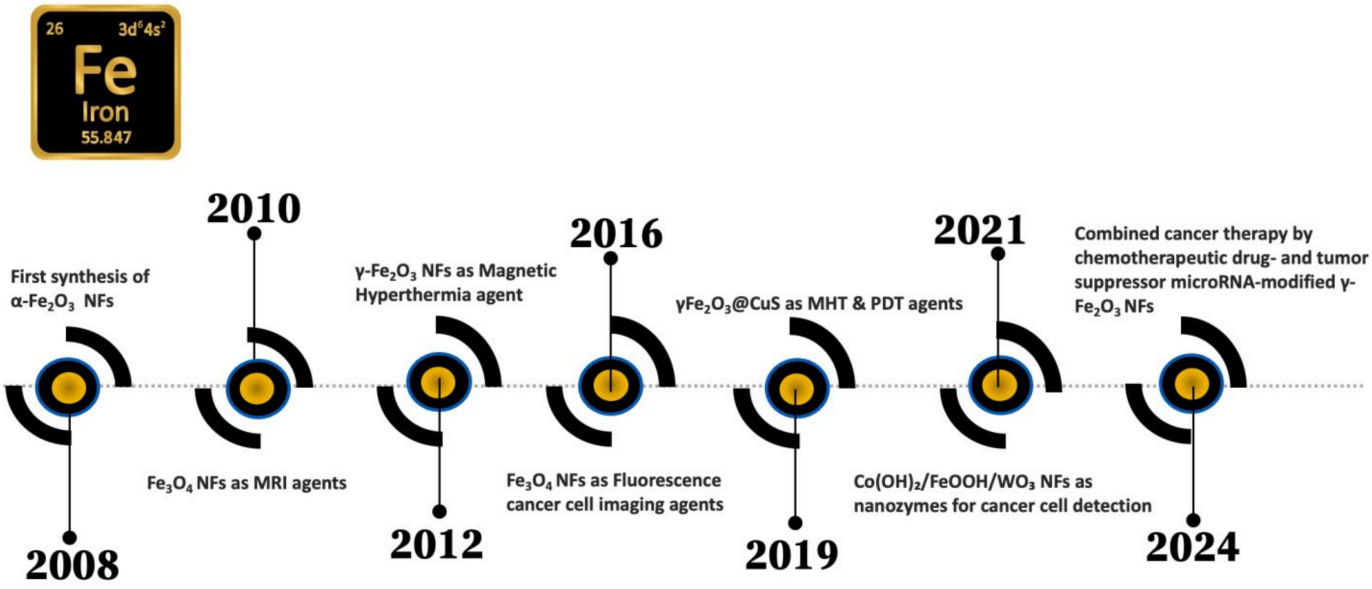
2. Synthesis Methods for Copper- and Iron-Based Nanoflowers

Ongoing research has focused on developing new synthesis methods for NFs [22]. Figure 1a,b presents key milestones in the history of copper- and iron-based nanoflowers.



(**a**)

Figure 1. *Cont.*



(**b**)

Figure 1. Key milestones in the history of (**a**) copper- and (**b**) iron -based nanoflowers.

As outlined by Kulkarni, nanomaterials are generally synthesized using physicochemical, biological, and hybrid methods [41]. Table 1 examines the advantages and constraints thereof.

Table 1. A summary of the main advantages and drawbacks of the synthesis method options.

Synthesis Method	Advantages	Drawbacks	Economic Considerations
Co-precipitation	The particles generated are relatively less toxic and simpler to produce [42]. The synthesis occurs at a lower temperature compared to other conventional methods [42]. This is a fast method [44].	Reactants need to have similar precipitation rates [34]. There are possible impurities in the product [34]. It requires waste management in non-aqueous solutions [34].	Low cost of chemicals [43].
Sol–gel	It has the ease of industrial scaling up [44]. It has high purity [45]. It has a uniform size distribution [48].	It produces a low yield [44]. It cannot be applied on a large scale [46]. This is a time-consuming process, includes several steps [49].	Low energy consumption due to mild temperature usage [47].
Hydrothermal	This is a non-toxic solvent, green method [50]. It enables the precise control of size and morphology [51].	We cannot observe the crystals through the process [34].	High cost of autoclave [34].
One-pot biomineralization	Immediate biomimetic mineralization simultaneously combines MNP preparation with surface functionalization [52]. This approach offers an eco-friendly and safe method for synthesizing multifunctional biomaterials, inspiring future researchers in the development of smart materials [52]. Additionally, the one-pot technique operates under gentler reaction conditions, is time-efficient, and aligns with the principles of sustainable development [52].	The produced material frequently exhibits low performance in technical applications, primarily due to relying on pre-existing natural pathways that have evolved over time [53].	Less expensive [52].
Sonochemical	This approach is an environmentally friendly option, and it operates fast without the need for high-temperature conditions [33].	Predicting the overall reaction mechanism is challenging as it depends on factors such as the type of reactor, the applied irradiation power and duration, and, most critically, the substrates and solvents used. Each material prepared using ultrasound requires the specific optimization of its synthesis conditions [54].	A cost-efficient approach [55].
Polyol	A high boiling point ensures the formation of well-crystallized materials [56]. Additionally, the reducing medium safeguards the freshly prepared metal particles from oxidation. Its ability to coordinate both metal precursors and particle surfaces enables precise control over the resulting structures and morphologies [57]. These features make it widely used in industrial applications [42].	It lacks the drawback of a low boiling point, which often necessitates the use of an autoclave [57].	Regarded as green and cost-efficient solvent [42]. Exhibits solubility for compounds similar to water, enabling the use of simple, inexpensive metal salts as starting materials [58].
Assisted by microwaves	It is considered a quick, simple, green approach [59].	It has pressure sensitivity and penetration depth [60]. There are challenges with scaling up [61]. Not all solvents are appropriate [61].	Cost efficiency [59].

The chemical synthesis of inorganic NFs similarly employs these established or modified techniques as illustrated in Figure 2.

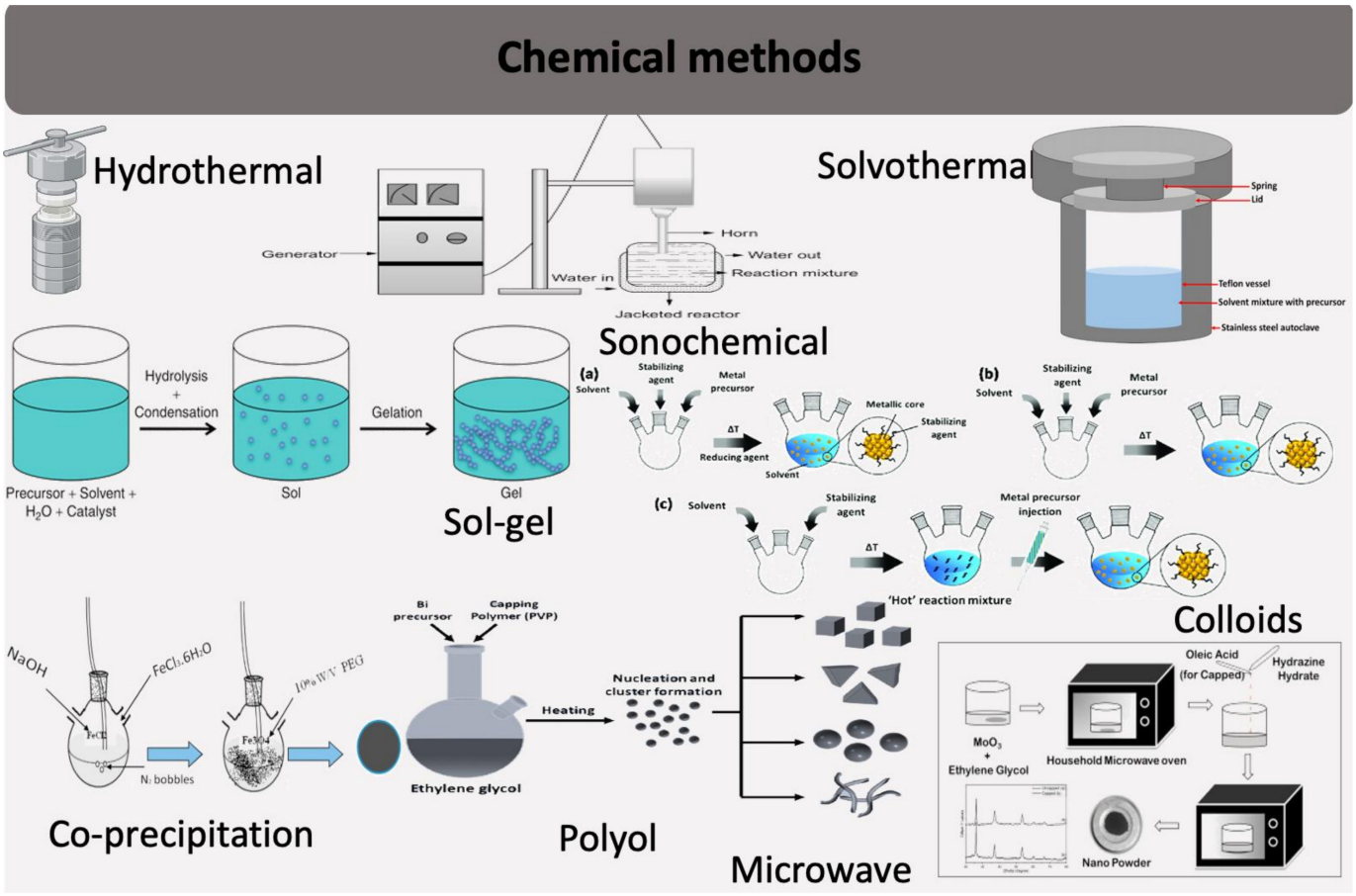


Figure 2. Commonly chemical employed techniques for synthesizing inorganic nanoflowers.

2.1. Co-Precipitation Method

Co-precipitation is the very frequently utilized in biomedical applications due to its ability to produce relatively less harmful and easily prepared particles [62]. Additionally, this approach offers safety and cost efficiency and operates at a lower temperature levels as opposed to alternative techniques [42].

The overall reaction of ferric and ferrous ions can be expressed as

$$Fe^{2+} + 2Fe^{3+} + 8OH^{-} \rightarrow Fe_3O_4 + 4H_2O.$$

If the reaction conditions are carefully controlled, it may oxidize to $Fe(OH)_3$, significantly impacting the properties of the NPs. This reaction can be represented as follows:

$$4Fe_3O_4 + O_2 + 18H_2O \rightarrow 12Fe(OH)_3.$$

Other reaction parameters, including the rate at which the solution is added and the stirring speed, also influence the quality of the result. It is essential to regulate the pH of the reaction mixture throughout both the synthesis and purification stages. Additionally, due to their high surface-to-volume ratio, nanoparticles have the tendency to aggregate in solution to minimize their surface energy. As a result, alternative approaches have been established to achieve better outcomes and more uniform dimensions [42].

Ganeshlenin Kandasamy et al., synthesized hydrophilic, surface-functionalized superparamagnetic iron oxide nanoparticles (SPIOs) for liver cancer treatment through magnetic fluid hyperthermia (MFH)-based thermotherapy. In calorimetric fluid hyperthermia

(C-MFH) studies, aqueous ferrofluid (AFF) based on SPIOs coated with 34DABA demonstrated a faster thermal response to an applied alternating magnetic field (AMF). Furthermore, the 34DABA-coated SPIO-based AFF exhibited superior heating efficiency, with specific absorption rate (SAR) and intrinsic loss power (ILP) values of 432.1 W gFe^{-1} and 5.2 nHm^2 kg^{-1}, respectively, at 0.5 mg mL^{-1}. The high heating efficiency of 34DABA-coated SPIOs is attributed to an enhanced π-π conjugation within the coating molecules and improved anisotropy from an SPIO cluster or chain formation in ferrofluid suspensions. These nanoparticles also exhibit excellent cytocompatibility over 24 and 48 h incubation periods and achieve a superior cancer cell killing efficiency of 61–88% against HepG2 liver cells through magnetic fluid hyperthermia (MFH), outperforming AMF- or water-bath-based thermotherapy alone [63].

Figure 3 shows the coating molecules and the chemical synthesis process for these surface-functionalized SPIOs [63].

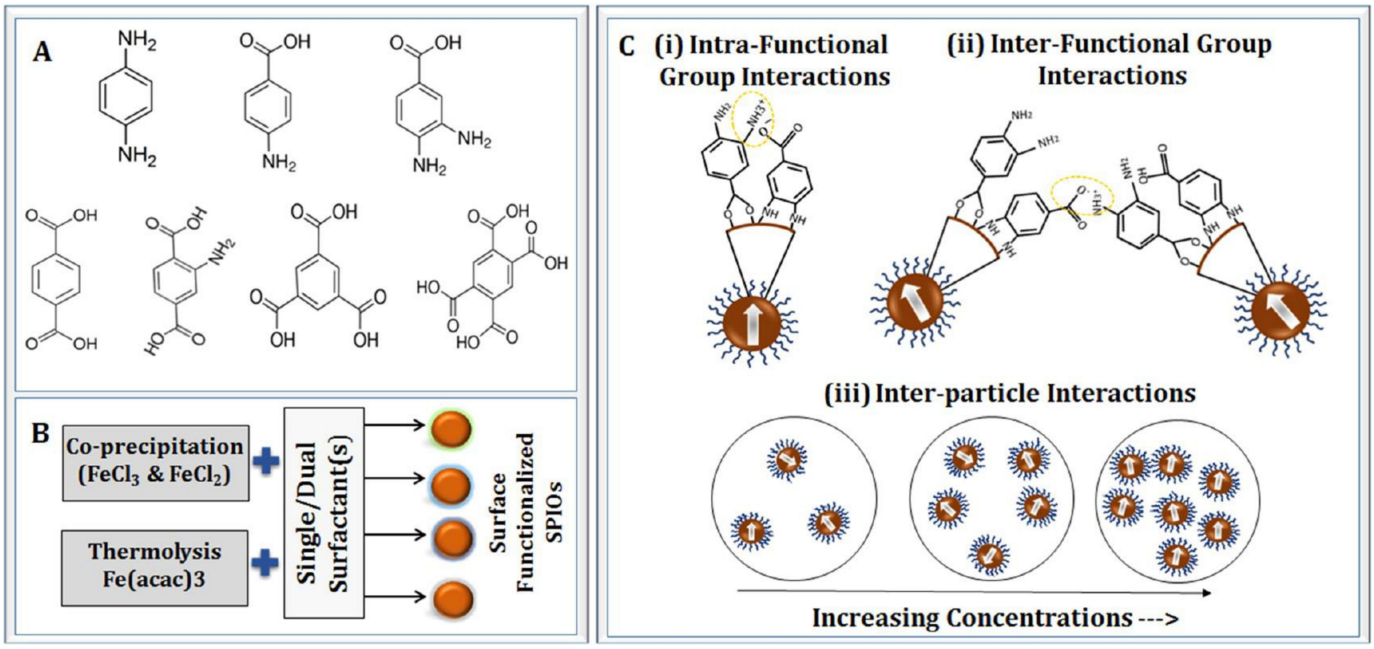


Figure 3. (**A**) shows the molecular structures of the surface coatings used on SPIOs; (**B**) provides a schematic of SPIO synthesis using single or dual surfactants through co-precipitation and thermolysis; and (**C**) illustrates interaction types in 34DABA-coated SPIO formulations. The interactions in these formulations are categorized as (**i**) intrafunctional and (**ii**) interfunctional groups, as well as (**iii**) interparticle interactions [63].

The produced SPIOs successfully entered the HepG2 liver cancer cells, as confirmed by Prussian blue staining. These SPIOs could be valuable in cancer thermotherapy [63].

Shahri et al., synthesized copper-molybdate ($CuMoO_4$) nanoflowers by employing the co-precipitation method. In their experiment, an aqueous solution of Copper Salicylidene ($Cu(Sal)_2$) in the presence of different surfactants was used as a precursor, while an aqueous solution of $(NH_4)_6Mo_7O_{24}$ $4H_2O$ was used as a precipitating agent. To investigate the effect of surfactants on the morphology and size of the product, SEM images were obtained for the prepared samples using polyvinylpyrrolidone (PVP), polyethylene glycol 600 (PEG), sodium dodecyl sulfate (SDS), and cetyltrimethylammonium bromide (CTAB) as surfactants. In a typical procedure, the two solutions were mixed and heated together. After that, the product was further processed by filtration, cleaning and drying [64].

2.2. Sol–Gel Method

The sol–gel process (Figure 4) is a widely used wet chemical method for synthesizing various nanostructures, especially metal oxide nanoparticles. In this technique, a molecular

precursor, typically a metal alkoxide, is dissolved in water or alcohol and undergoes hydrolysis or alcoholysis through heating and stirring, leading to condensation and the formation of a gel. Since the gel remains wet, it requires drying, which is tailored to achieve specific properties and applications. For example, in an alcoholic solution, drying may involve burning off the alcohol. After drying, the gel is powdered and calcined. This conventional and industrially relevant method enables the synthesis of nanoparticles with diverse chemical compositions. The process begins with forming a homogeneous sol from precursors, which transitions into a gel. During the drying stage, the solvent is removed, and the properties of the resulting dried gel are significantly influenced by the selected drying technique [65].

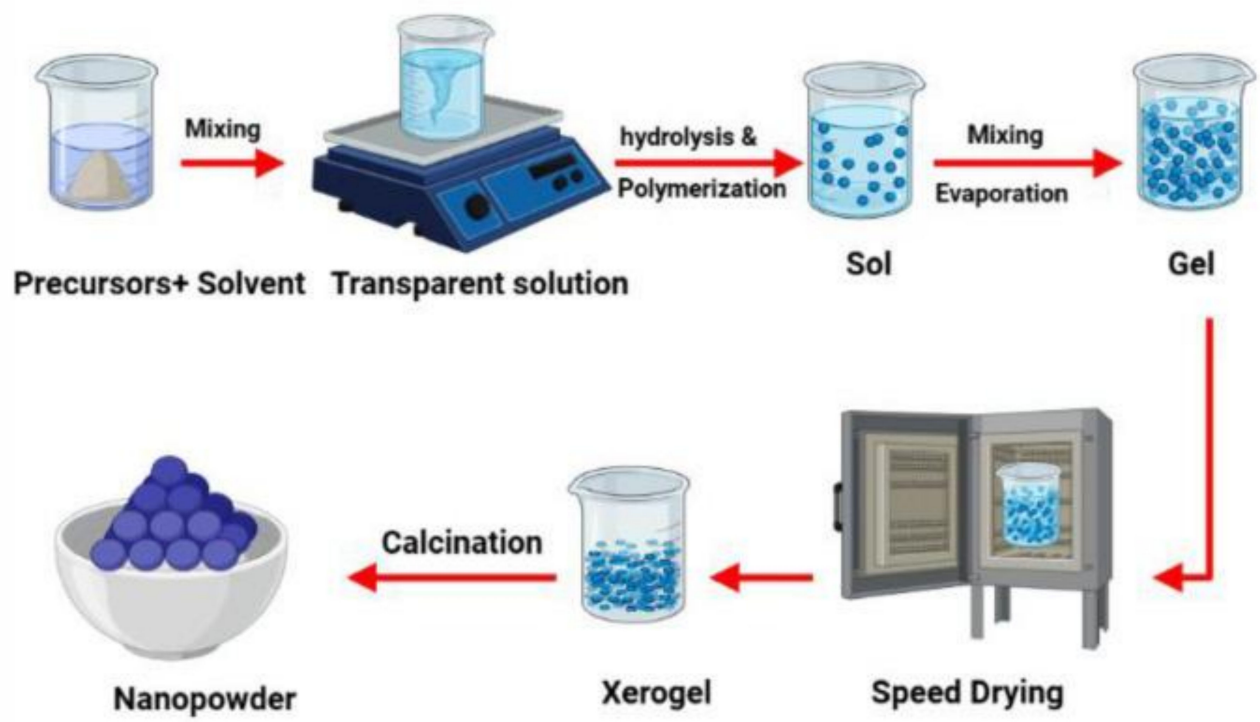


Figure 4. Illustration of the sol–gel process for synthesizing nanomaterials. Reproduced with permission from Ref. [66].

Due to its simplicity, the sol–gel method is also commonly used in NF production. Sol is a type of colloidal suspension of solid particles in a liquid, while gel is a viscous 3D macromolecular network immersed in a solvent [34]. This process includes five stages: hydrolysis, polycondensation, aging, drying and calcination [33]. The first three steps are related to the gradual formation of the gel structure, while the other two are associated with the separation of aqueous and organic components and the removal of water molecules, respectively [34]. The sol–gel method produces MNPs with high purity and uniformity; however, it can also lead to impurities that are challenging to remove. Like other techniques, it offers substantial control over particle size and composition [42].

2.3. Hydrothermal Method

Hydrothermal synthesis involves the reaction of a solid substance with an aqueous solution at an elevated temperature and pressure within a reaction vessel, resulting in the deposition of fine particles [67]. This method is solution-based, with water serving as the solvent, hence the term "hydrothermal" [68]. This process takes place in a steel pressure vessel called an autoclave, where temperature and pressure are carefully regulated. The temperature is raised above the boiling point of water until vapor saturation is reached [69]. The hydrothermal method has played a crucial role in modern science and technology due to its advantages, including uniform precipitation, low cost, scalability, and the production

of a pure final product [34]. Furthermore, the hydrothermal technique encompasses various applications, including hydrothermal synthesis, treatment, crystal growth, organic waste treatment, and the preparation of functional ceramic powders [70].

The hydrothermal method, widely used for nanoparticle synthesis, facilitates rapid nucleation and growth at various temperature and pressure levels [42]. This eco-friendly, cost-effective, and versatile approach yields pure nanoparticles with a specific morphology [71] without needing organic solvents or additional post-synthesis treatments [72,73]. However, its limitations include an inability to produce particles smaller than 10 nm and slow reaction kinetics at high temperatures. Despite its limitations, the hydrothermal method provides excellent magnetic controllability and superior control over particle size, shape, and dispersion compared to alternative techniques [74].

Jiamin Sun and colleagues created a nanoflower-based therapeutic using iron ions, thioguanine (TG), and tetracarboxylic porphyrin (TCPP) through a one-step hydrothermal process for chemo/chemodynamic/photodynamic cancer therapy. The resulting nanoflowers, featuring a low-density Fe_2O_3 core and a shell of iron complexes (Fe-TG and Fe-TCPP), show strong tumor site accumulation, favorable degradability within the tumor microenvironment (TME), the effective inhibition of tumor growth and metastasis, and the ability to boost host antitumor immunity [75].

In the acidic tumor microenvironment, the nanoflowers degrade gradually after internalization, enabling targeted drug release and catalytic reactions specifically at tumor sites. After treatment, iron ions are excreted via renal clearance. This multimodal therapy enhances antitumor immunity effectively without added toxicity. The degradable and easily manufactured nanomedicine shows strong potential for clinical precision oncology [75].

Yunfei Yan et al., synthesized hollow spherical and nanoflower Fe_3O_4 structures to improve magnetothermal conversion efficiency. Using the hydrothermal method, they achieved nanoparticles with a uniform size and shape distribution. The Fe_3O_4 nanoflowers exhibited a significantly higher intrinsic loss power (ILP) of 6.52, 1.83 times greater than that of hollow spherical Fe_3O_4 (3.55), demonstrating their strong potential for magnetic hyperthermia therapy (MHT) in cancer treatment [76].

Intrinsic loss power (ILP) measures a material's inherent ability to convert magnetic energy into heat in an alternating magnetic field, highlighting its intrinsic properties and efficiency. Because ILP is unaffected by external magnetic field parameters, it allows for unbiased comparisons across various magnetic nanomaterials, facilitating the identification of optimal candidates for magnetothermal applications [76]. The ILP is expressed as

$$ILP = \frac{SAR}{f\,H^2}$$

where the f represents the frequency of the alternating magnetic field, and H is its amplitude.

The synthesized Fe_3O_4-SC nanoflower nanoparticles demonstrated high ILP values compared to other magnetic materials. Specifically, Fe_3O_4 nanoflower-SC showed an 83.66% improvement over hollow Fe_3O_4 and a 10.70% increase over regular Fe_3O_4 nanoflowers. Additionally, incorporating dispersants into Fe_3O_4 nanoflowers reduced agglomeration, further enhancing their magnetothermal performance [76]. Despite these advantages, $Mn_{0.5}Zn_{0.5}Fe_2O_4$ nanoparticles [77] outperform hollow Fe_3O_4 in ILP, benefiting from Mn^{2+} doping, which optimizes magnetothermal performance.

Ying Xu and colleagues developed nanoflower-like Bi_2CuO_4 via a one-step hydrothermal method, leveraging its large surface area to adsorb aptamers and create a signal probe in a sandwich structure on the sensing interface. This enabled enhanced electrochemical signal detection and amplification. The resulting ratiometric biosensor, using Al-MOF, Ce-MOF, and Bi_2CuO_4, achieved an ultra-sensitive detection of HER2 within 0.001–20.0 ng/mL and can detect other tumor markers by altering the aptamer type, showing high universality and promising clinical application potential [78].

The synthesis of copper bismuth oxysulfide (BiCuOS) nanoflowers (NFs) using oleylamine and sodium citrate as a surfactant and a reducing agent in a one-step hydrothermal process was reported. The nanoflowers consist of bismuth oxide nanoplates arranged in nanoarrays on CuS bases, which enhances optical absorption under NIR light. With a point of zero charge (PZC) near the acidic tumor pH (~5.5), these BiCuOS NFs can absorb NIR light to induce hyperthermia in cancer therapy and act as laser cavity mirrors. Additionally, they can carry chemotherapeutic drugs like doxorubicin, enabling combined chemo-photothermal therapy for improved anticancer efficacy [79].

Hima Patel et al., investigated iron oxide-based magnetic nanoflowers in an in vitro study on breast cancer cells (MDA-MB-231). These monodispersed, temperature-sensitive nanoflowers, synthesized via hydrothermal methods, were tested for magnetic fluid hyperthermia (MFH) effects. The results showed that MFH, in the presence of magnetic nanoclusters, killed nearly 87% of cancer cells within 30 min, highlighting nanoflowers as a promising alternative to traditional single-domain magnetic nanoparticles for cancer treatment [80].

Negar Alizadeh and colleagues synthesized $Co(OH)_2/FeOOH/WO_3$ nanofibers (NFs) using a one-step hydrothermal method, demonstrating dual-function enzyme activity with enhanced peroxidase and catalase-like properties. The interactions between the NFs and hydrogen peroxide (H_2O_2) were studied using EPR, XPS, and UV-vis techniques. The NFs exhibited pH-dependent activity: peroxidase-like at acidic pH and catalase-like at basic pH. At acidic pH, they generated hydroxyl radicals, while at basic pH, they produced oxygen. The production of hydroxyl radicals and oxygen varied with NF concentration. The study also assessed their anticancer potential for photodynamic therapy (PDT) based on catalase-like activity and oxygen production. This work paves the way for the development of active nanozymes for biosensors and cancer therapy [81].

2.4. Polyol Process

After nearly thirty years of development, the polyol process has become a widely recognized and effective soft chemical method for synthesizing nanoparticles used in key technological areas. Polyols, along with traditional reducing agents, have proven to be highly efficient in producing metal nanoparticles, leading to the term "polyol process" [56]. First introduced in the late 1980s by Fiévet, Lagier, and Figlarz, this colloidal chemistry method allows for the liquid-phase synthesis of finely divided metals from their oxides, hydroxides, or salts using polyols [57]. Magnetically induced hyperthermia has also advanced significantly, now reaching phase III clinical trials for cancer treatment.

The polyol method is particularly favored for synthesizing flower-like magnetic nanoparticles (Figure 5), with substantial research focused on enhancing their magnetic heating capabilities. Improvements to the polyol process, such as controlling nanoparticle size and morphology through precise water addition or seeded growth methods, have been explored. It has been suggested that the polyol method offers more versatility than thermal decomposition, allowing better control over both particle size and the composition of the grains in the flower-like structures [82].

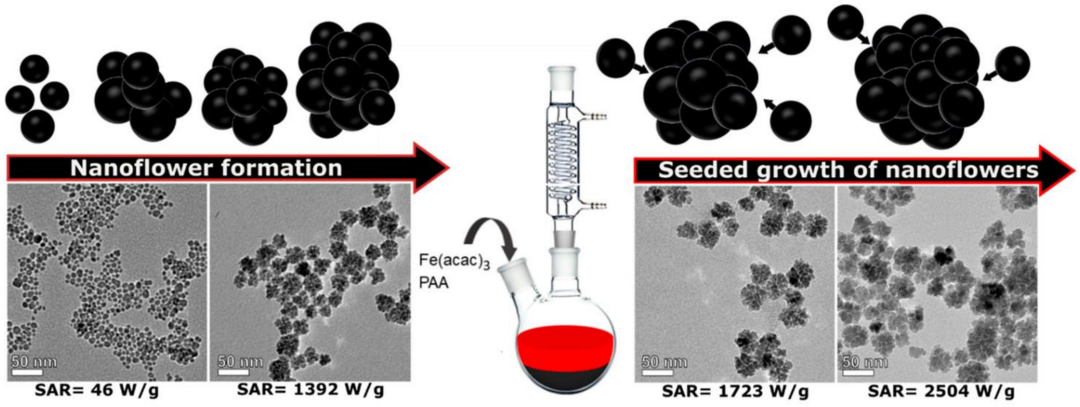


Figure 5. Synthesis of stable iron oxide nanoflowers with simple and fast polyol synthesis. Reprinted (adapted) with permission from Ref. [22]. Copyright 2021 American Chemical Society.

Liudmyla Storozhuk et al., developed a fast and simple method for producing colloidally stable iron oxide nanostructures with excellent heating capabilities using the polyol process. This approach led to biocompatible single-core nanoparticles and nanoflowers. The study optimized nanoparticle heating rates by adjusting parameters like precursor concentration, polyol molecular weight, and reaction time. Polyacrylic acid facilitated the formation of efficient nanoheating agents—iron oxide nanoflowers (IONFs)—in just 30 min. The seeded growth method enhanced nanoflower size, improving heating efficiency with an intrinsic loss parameter of 8.49 nH m^2 kg Fe^{-1}. The colloidal stability of the nanoflowers was preserved through a ligand exchange protocol, where polyol ligands were replaced with sodium tripolyphosphate for long-term stabilization (Figure 6) [22].

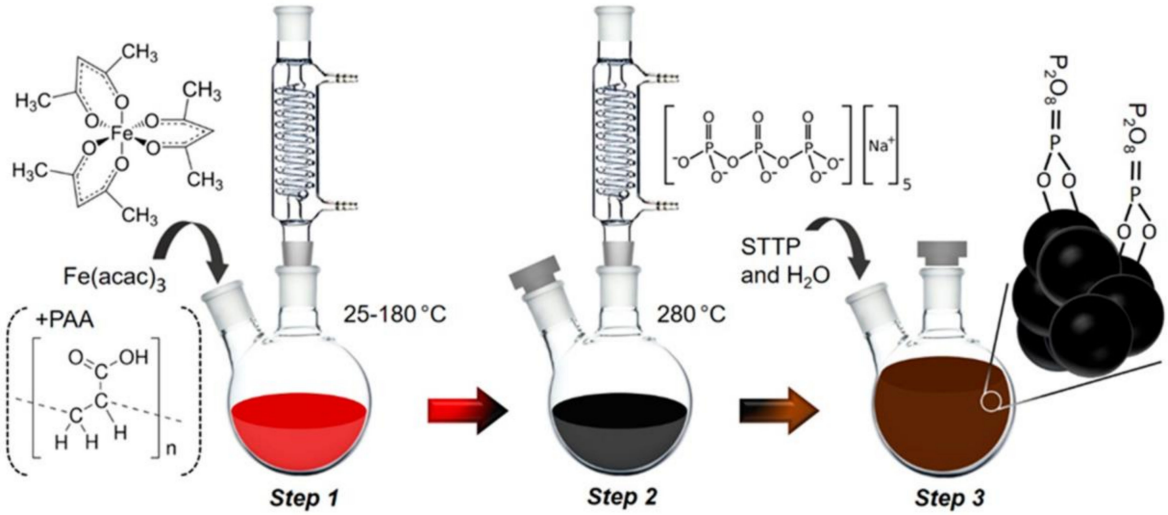


Figure 6. A schematic illustrating the simple one-pot thermal decomposition of $Fe(acac)_3$ in polyol synthesis is provided. In Step 1, single-core iron oxide nanoparticles (IONPs) are produced without poly(acrylic acid). In Step 2, iron oxide nanoflowers (IONFs) are formed with poly(acrylic acid). Finally, in Step 3, the stability of the resulting products in water is achieved by replacing the polyol ligand with sodium tripolyphosphate. Reprinted (adapted) with permission from [22]. Copyright 2021 American Chemical Society.

Maria Theodosiou et al., synthesized iron oxide nanoflowers (IONFs) as innovative heating mediators for magnetic hyperthermia therapy (MHT) using the polyol method. The resulting NFs exhibited cluster-like geometry, providing excellent colloidal stability and high specific absorption rate (SAR) values. The study compared NFs of different sizes and coatings, focusing on stability, magnetothermal responsiveness, and in vitro behavior,

including cytotoxicity and cellular localization, both with and without MHT. To facilitate simultaneous cellular imaging and therapy, the nanoflowers were coated or loaded with Rhodamine B (RhB), a red fluorescent dye with high quantum yield and photostability. The research also compared the in vitro behavior of RhB-loaded NFs and magnetoliposomes to assess their therapeutic and imaging potential under MHT [22,83].

2.5. Microwave-Assisted Method

Microwave irradiation offers a fast and efficient environment for synthesizing nanomaterials due to its uniform and controlled heating properties. Consequently, microwave-assisted synthesis methods have garnered significant attention in the literature [33].

Microwave-based synthesis enhances nucleation and growth through microwave irradiation, enabling swift nanoflower production [32]. When combined with hydrothermal synthesis, the microwave process requires significantly less power and time, allowing for the synthesis of nanomaterials at lower temperatures compared to traditional furnace heating. The conventional hydrothermal method for nanomaterial synthesis typically involves long reaction times and high energy consumption, whereas the microwave-assisted approach provides faster heating, higher yields, and an improved reproducibility of the nanocrystals. Thus, utilizing microwave energy for chemical reactions offers substantial advantages, as it is a straightforward, highly efficient, and environmentally friendly process [84].

S.K. Shaw et al., studied the microwave-assisted polyol method to synthesize γ-Fe_2O_3 nanoflowers. By adjusting the amount of sodium acetate as an alkali source, they were able to modify the structural and magnetic properties, leading to nanoflowers with excellent heating performance in magnetic hyperthermia therapy (MHT) and photothermal therapy (PTT). Photoluminescence spectroscopy revealed the role of defects, such as oxygen vacancies and surface states, in enhancing the performance. The γ-Fe_2O_3 nanoflowers exhibited improved crystallinity, a higher coercive field, and an intrinsic loss power value of 15.21 ± 0.34 nHm^2/kg, which was significantly higher than commercially available ferrofluids and other nanoflowers. During PTT, a therapeutic temperature of 42 °C was reached at a concentration as low as 100 µg/mL, demonstrating the effectiveness of γ-Fe_2O_3 nanoflowers as a PTT agent [85].

2.6. Sonochemical Method

The sonochemical method is another technique for producing NFs, utilizing ultrasonic waves (Khorsand Zak et al., 2013 [86]). This environmentally friendly approach avoids the use of highly toxic chemicals and does not necessitate high-temperature conditions. By optimizing the energy of the ultrasonic waves and the exposure duration, desired shapes and yields of nanomaterials can be achieved [33]. This method offers several advantages, making it a leading technique: it is simple, environmentally friendly, cost-effective, and safe. The chemical and physical effects of ultrasound are not caused by direct interactions between chemical species and sound waves but rather by the physical phenomenon of acoustic cavitation. This process involves the formation, growth, and eventual explosive collapse of bubbles in the liquid. These stages generate localized hot spots with temperatures around 5000 °C and pressures of 500 atm, lasting only a few microseconds. Consequently, when a liquid is exposed to high-intensity ultrasound, high-energy chemical reactions are triggered [87]. The sonochemical method induces intense local heating, high pressure, and extremely rapid cooling rates, all due to acoustic cavitation—the continuous formation, growth, and implosive collapse of bubbles in the liquid [88].

The sonochemical method was developed to further optimize the one-pot method and facilitate even more HNF production. The use of a sonicator bath accelerates the formation of HNFs from three days of incubation to under ten minutes. In a similar way, Gulmez et al., used a $CuSO_4$ $5H_2O$ solution and a hemoglobin solution and incubated their mixture with sonication for ten minutes [89]. In both cases, the refining of the produced HNFs was

carried out according to the conventional method. It should be noted that enzyme-free HNFs, containing the typical inorganic part (metal phosphates) and an organic part (pieces of DNA sequence or antigens but not enzymes), are considered to be the second generation of HNFs [90] and are generally synthesized with similar methods as the ones mentioned above [91,92].

2.7. Biomolecule Immobilization

In recent years, extensive research has concentrated on the development of biomolecule-integrated nanostructures for a range of potential applications in biomedical sciences. Many of these approaches utilize enzymes (Figure 7), which are known for their exceptional activity and specificity. However, like most biomolecules, they are highly susceptible to various environmental factors. To enable their application in large-scale reactions across different industries, enzymes have been immobilized. This immobilization enhances their stability, reusability, and enantioselectivity while simplifying product purification, making them a more economically viable option [93]. As a result, the immobilization of enzymes has garnered significant interest from researchers and the scientific community due to their extensive range of applications [94].

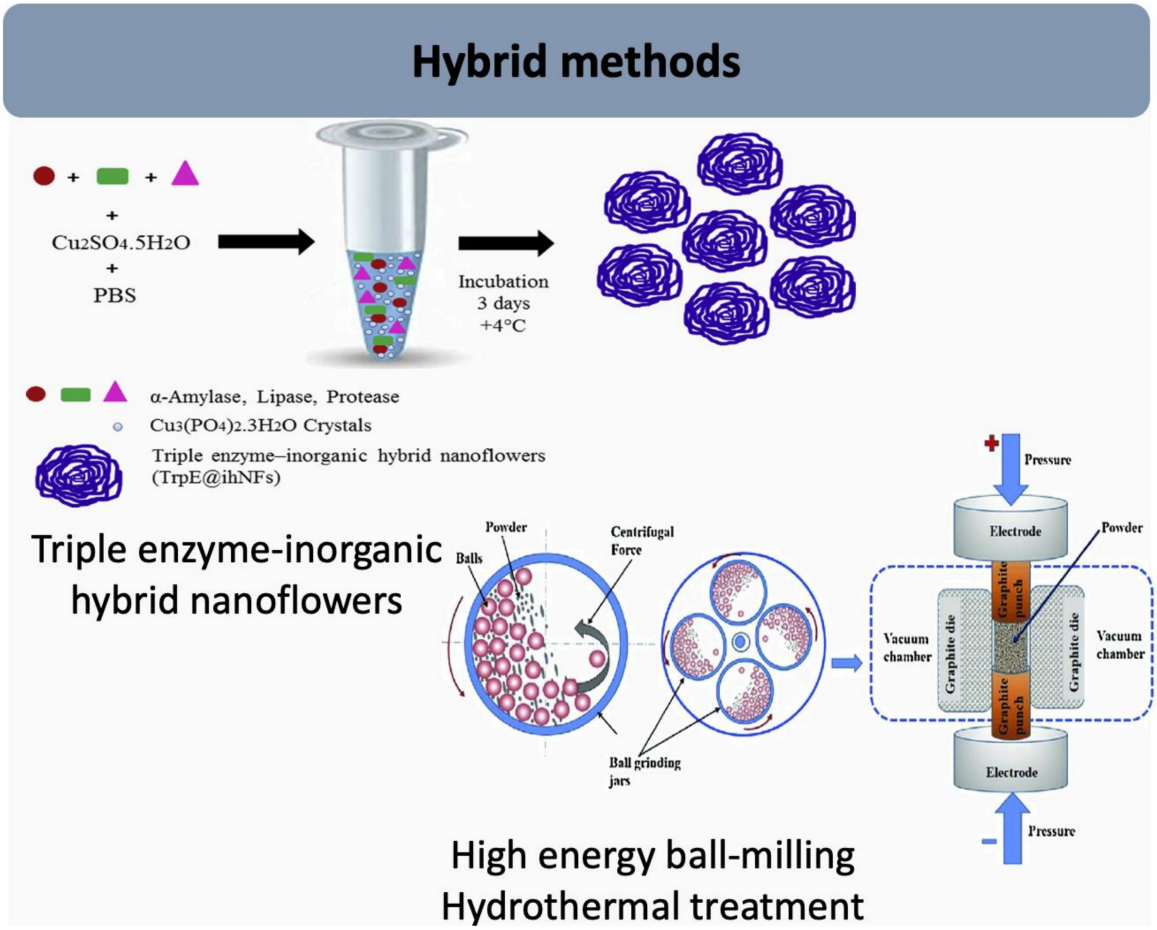


Figure 7. Hybrid employed techniques for synthesizing inorganic–organic nanoflowers.

The concept of biomolecule-embedded nanomaterials, where biomolecules are immobilized within nanostructured materials, is a promising area of research that improves the stability, activity, and selectivity of the biomolecules. Traditionally, biomolecules have been covalently bonded, trapped, or physically adsorbed onto various supports like bulk materials, beads, membranes, and fibers. However, improper immobilization can reduce biomolecule activity due to issues like blocked active sites, mass transfer limitations, and

conformational changes. Recently, organic–inorganic hybrid nanoflowers and biomolecule-encapsulated metal–organic frameworks (biomolecule@MOF (CD BioSciences, Shirley, NY, USA)), formed through self-assembly, have attracted significant attention in this field.

These composites provide a straightforward synthesis, high efficiency, and considerable potential to enhance the stability, activity, and selectivity of biomolecules, outperforming traditional immobilization methods. Biomolecules, such as proteins, strongly bind to metal ions, mainly through the coordination of amide groups in the protein backbone [95].

Duygu Aydemir et al., synthesized triple enzyme–inorganic hybrid nanoflowers (TrpE@ihNFs) by combining α-amylase, lipase, and protease with Cu^{2+} ions. They compared the enzyme activity and stability of TrpE@ihNFs with those of the free enzymes under varying pH levels and temperatures using spectrophotometric methods. The results showed that the enzyme activities and stability of TrpE@ihNFs were significantly superior to those of the free enzymes [96].

2.8. One-Pot Biomineralization

Biomineralization, the process by which biological systems produce inorganic materials, has become an attractive method for sustainably creating functional nanomaterials. Relying on proteins or other biomolecules, this process occurs at ambient temperatures and pressures, offering a scalable, cost-effective, and environmentally friendly approach to nanoparticle synthesis [53].

Biomineralization is a natural process used by various organisms to produce functional inorganic crystals with complex hierarchical micro- and nanostructures. Biomolecules, particularly proteins, act as templates that guide the assembly of inorganic nanomaterials, forming structures like bones, teeth, shells, and fish scales. Collagen, the most abundant protein in animals, has a unique triple-helix structure made of repetitive amino acid sequences. Its rod-like structure and self-assembly properties make it a strong building block, making collagen the primary biotemplate for synthesizing inorganic mesocrystals in the human body [97].

Figure 8 illustrates the stepwise fabrication of milk allergen, β-lactoglobulin biosensor on polyimide (PI) film.

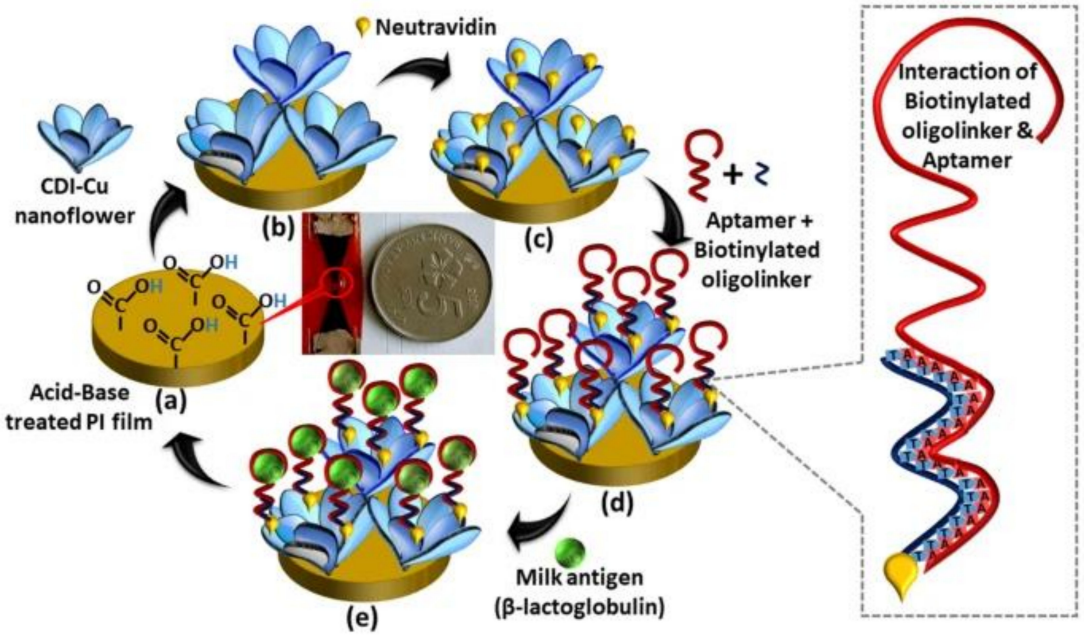


Figure 8. Stepwise fabrication of milk allergen, β-lactoglobulin biosensor on polyimide (PI) film involves the following steps: (**a**) acid–base treatment to introduce carboxylic functional groups, (**b**) deposition of CDI-Cu hybrid nanoflowers (NF), (**c**) modification with neutravidin, (**d**) immobilization of oligoaptamer, and (**e**) detection of β-lactoglobulin [98].

The innovative biomimetic mineralization strategy known as the one-pot method enables the direct and efficient synthesis of smart biomaterials with multiple responsive capabilities in an environmentally friendly manner. This one-pot approach is simpler to operate, does not necessitate oxygen isolation, and features milder and faster reactions, resulting in reduced environmental and operator harm. This aligns with the principles of green chemistry in the preparation of multifunctional magnetic nanoparticles [52].

2.9. Biological Method/Green Synthesis

The green synthesis of metal nanoparticles (Figure 9) has received notable attention, especially in medicine [99].

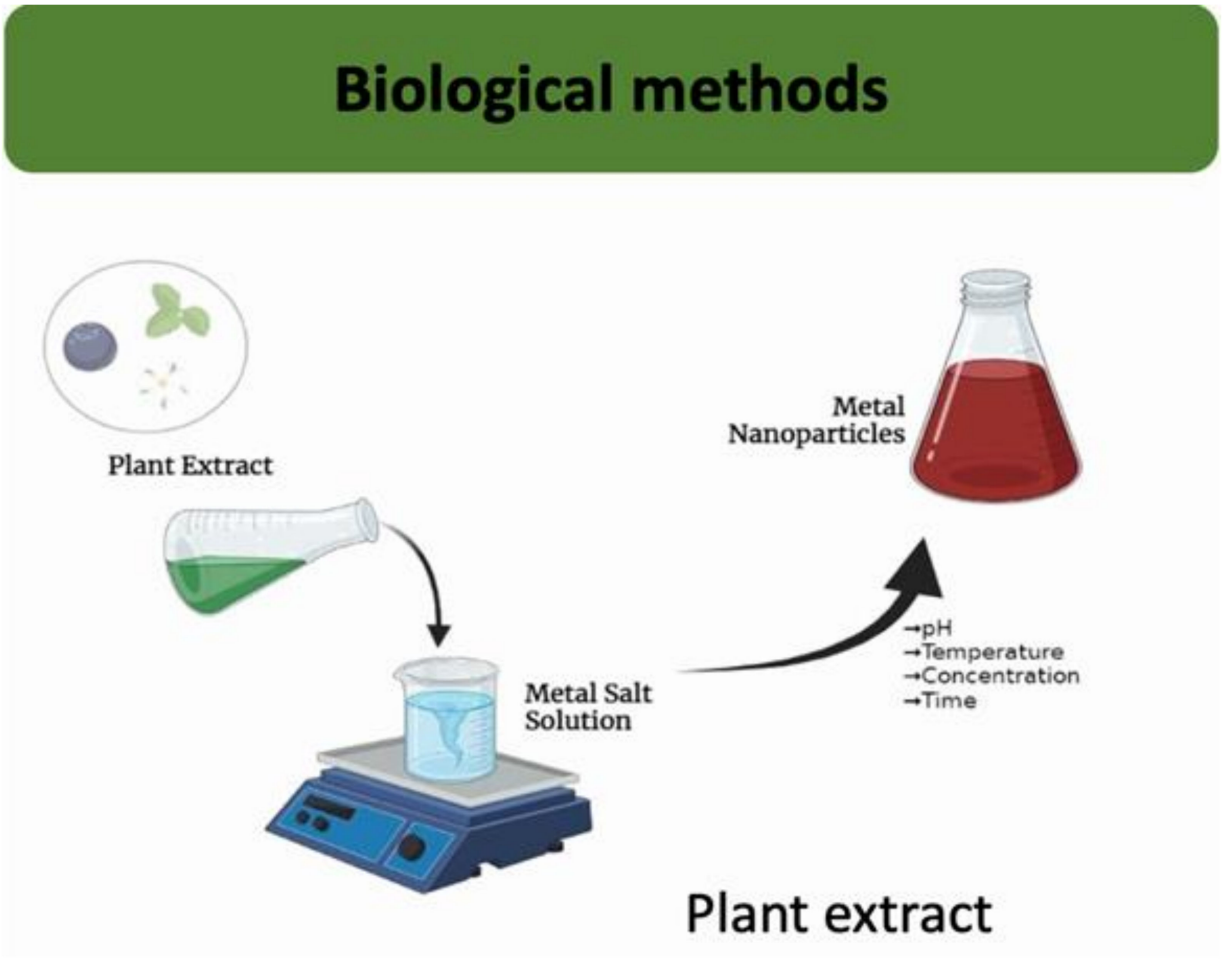


Figure 9. Biological employed techniques for synthesizing inorganic nanoflowers.

Green synthesis is considered a better approach because traditional methods often rely on hazardous chemicals and require significant energy inputs, both of which have negative environmental impacts. In contrast, green synthesis employs natural sources such as enzymes, plant extracts, microbes, or biocompatible agents for the synthesis process. Using biomolecules and plant extracts to synthesize nanoflowers ensures environmentally friendly practices while also introducing biocompatibility, which is crucial for biomedical applications [32]. The utilization of plant extracts for producing metal nanoparticles is favored for its simplicity, scalability, and non-toxicity [100]. However, the application of this approach for synthesizing NFs is still in its early phase, with only a few works exploring this specific method.

A green synthesis process has been proposed for creating HNFs using Cu(II) and Co(II) metal ions as inorganic components, along with quercetin as the organic component. When evaluating the anticancer activities of HNFs, it was found that CuHNFs exhibited more effective anticancer properties compared to quercetin and CoHNFs, depending on concentration levels. Specifically, CuHNFs led to 80% cell death, while ZnhNFs resulted in 30% cell death, and quercetin caused 40% cell death. These observations clearly demonstrate that cell death is concentration-dependent [101].

A green synthesis mechanism was developed using *Tribulus terrestris* L. extract as the organic component along with copper, zinc, and cobalt metal ions. Cytotoxic evaluations indicated that cobalt nanoflowers may be a safer therapeutic option compared to other plant extracts and nanoflowers. To synthesize *T. terrestris*-Cu nanoflowers (CuHNFs), a stock solution of $CuSO_4$ $5H_2O$ at 120 mM was prepared and mixed with 8 mL of 10 mM phosphate-buffered saline (pH 7.4). The plant extract was then added at a concentration of 0.02 mg/mL. The mixtures were incubated at +4 °C for 72 h, followed by centrifugation at 10,000 rpm for 20 min. The hybrid nanoflowers were finally dried at room temperature (Figure 10) [102].

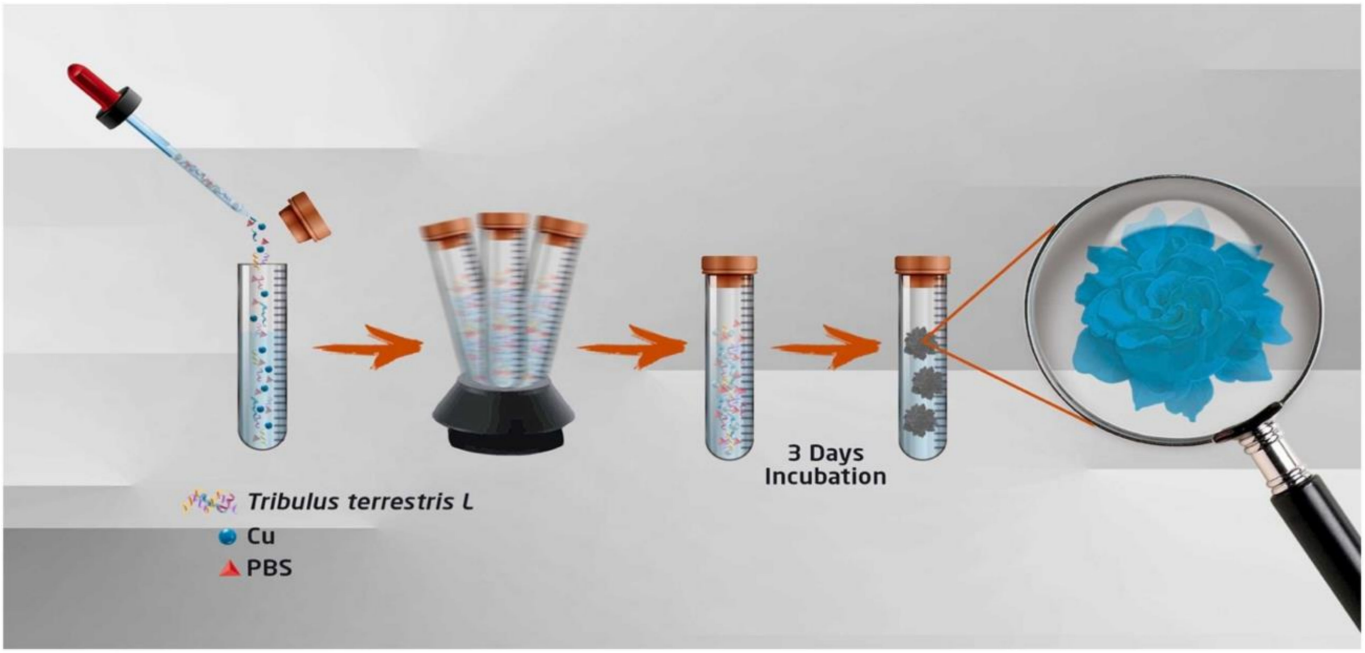


Figure 10. *T. terrestris* L.-Cu(II) hybrid nanoflowers (*T. terrestris* L.-CuhNFs) synthesis scheme. Reproduced with permission from Ref. [102].

The zinc and copper hybrids had a notable impact on cell lines up to a specific concentration, beyond which they increased cell viability. Furthermore, all hybrids demonstrated improved anticancer activity compared to the extract. These results could contribute to the development of effective new-generation formulations for treating A549 lung cancer [102].

3. Experimental Parameters' Effect on Morphology of Nanoflowers

The morphology of NFs and HNFs, and therefore their efficacy (Table 2), is affected by many variables such as temperature, pH and time of incubation.

Table 2. Parameters affecting morphology of nanoflowers.

Parameter	Effect on Morphology	Reference
pH	Depending on pH conditions during synthesis, fully grown, semi-developed and non-developed NFs and HNFs can be obtained	[103,104]
Temperature	The temperature window range favoring HNF formation depends on material composition and synthesis process	[104]
Incubation time	NF and HNF growth lasts for about 72 h until they "blossom"	[104,105]
Immobilization of multiple enzymes	enhancing their biodistribution by increasing the NP's water solubility	[83]

3.1. Effect of pH

Xiang et al., studied the effect of pH on the morphology of CuO nanostructures. In their report, they concluded that a pH value equal to 10.5 is optimal for the formation of NFs [106]. Hao et al., investigated the role of pH conditions on the synthesis of self-assembled *Brevibacterium* cholesterol oxidase enzyme-containing Cu(II) HNFs (COD-Cu) and found that the optimum value for their formation was pH = 7, and for pH equal to 5 and 3, smaller-sized and not fully grown flower-like structures were obtained, while at pH = 9, no HNFs were formed [104].

Concerning the production of HNFs, the pH of the reaction system directly affects the net charge of biomolecules, influencing their affinity to metal ions or other biomolecules, so typically, the pH value should be carefully selected according to the isoelectric point (pI) [105,107]. A pH value lower than the pI can result in repulsion between metal ions and enzymes, while a value equal or higher than the pI can result in a neutral or negative overall change, thus facilitating the formation of NFs. Therefore, this variant has a significant effect on the morphology and properties of the immobilized enzyme. Gao et al., synthesized copper-based HNFs, changing the parameter of the pH (ranging from 7.0 to 8.5) of the buffer solutions in order to test the morphology of the produced HNFs [103]. According to their results, pH values further from the isoelectric point (pI) resulted in a regular HNF morphology and larger flower-like nanocrystals.

3.2. Effect of Temperature

Moderate temperatures are usually required both in the synthesis of NFs and HNFs. Sahri et al., investigated the effect of temperature on the final morphology of $CuMoO_4$ NFs [64]. The formation of $CuMoO_4$ NFs took place at a narrow temperature window around 35 °C, and at higher temperatures, underdeveloped and deformed NFs were produced, while at lower temperatures no NFs were formed. On the other hand, self-assembled COD-Cu HNFs can be obtained at a wider temperature range (4–25 °C), with their size and "petal" density increasing with temperature. However, at 37 °C, stacked "petals" rather than spherical flower-like structures were observed [104]. It should also be noted that the HNF system's functionality is not always proportional to the morphology of the petals. Because of their nature, each enzyme shows optimal activity at its own temperature.

3.3. Effect of Incubation Time

Typically, NF and HNF growth lasts for about 72 h until they "blossom". For instance, after the first 24 h of incubation, tiny COD-Cu spheres were obtained, some individual "petals" appeared after 48 h, and fully grown HNF structures were formed after the overall 72 h (Figure 11c) [104].

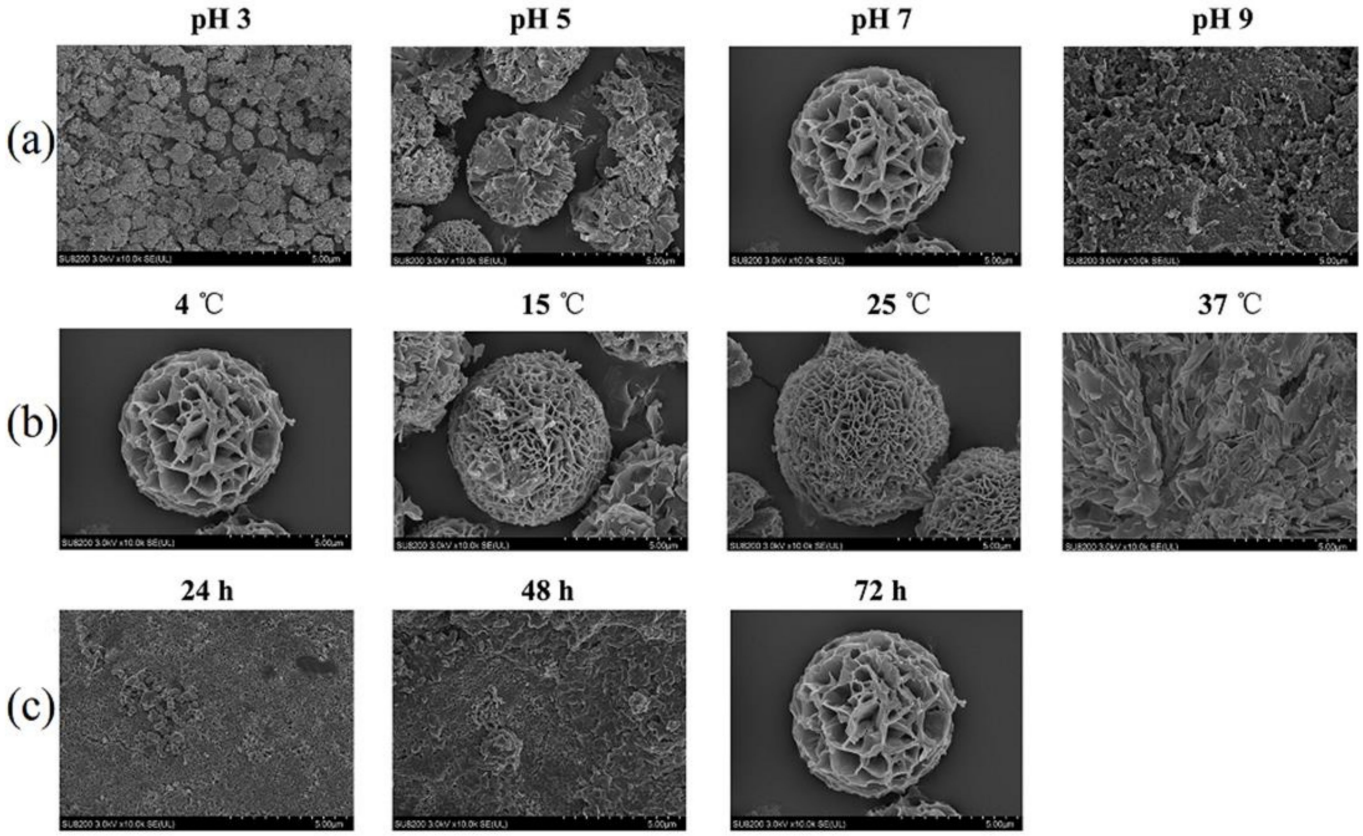


Figure 11. FE-SEM images of enzyme-functionalized Cu(II) HNFs. Effect of (**a**) pH, (**b**) temperature, and (**c**) incubation time on their morphologies. Modified and reproduced with permission from Ref. [104].

It is worth noting that overgrowth will reduce the activity of biomolecules in HNFs, resulting in a decline in catalytic efficiency [105]. Therefore, the sonochemical method is more beneficial for the production of NFs and increases the time period of their storage.

4. Synthesis Methods and Applications of Flower-like Copper- and Iron-Based Nanostructures

4.1. Iron-Based NFs

Iron oxide NPs have been examined for their safety, biocompatibility, and significant clinical applications over the years. Various methods exist to activate their therapeutic properties, with superparamagnetic iron oxide nanoparticles (SPIONs) being particularly notable for their use as MRI contrast agents due to their non-toxic nature and the lack of residual magnetic force once the external field is removed. Transition metals or metal oxides are often selected for their high magnetic saturation to enhance therapeutic effectiveness. Magnetite (Fe_3O_4) and maghemite (γ-Fe_2O_3) nanoparticles have diverse biomedical applications, including drug delivery and cancer treatment. Their non-toxicity, biocompatibility, and relative ease of functionalization with various polymers or functional groups further enhance their utility [42]. Conventional Fe_3O_4 nanoparticles are typically synthesized using a hydrothermal method without modifications, which frequently results in particle aggregation and precipitation. To address this issue, surface modifications and coatings are commonly employed to enhance the stability of Fe_3O_4 nanoparticles. Mesoporous silica is often used as a material for surface passivation [108].

Iron NFs, along with other ferrous-based nanoparticles, are currently studied to be used in cancer theranostics, due to their excellent magnetic properties [76]. As an imaging modality, iron-based NFs have an auxiliary role as contrasting agents in MRI scans both in in vitro and in vivo experiments. Concerning cancer therapy, NFs find use in PTT. Usually,

PTT is based on photothermia: the optical excitation of plasmonic nanoparticles by an infrared laser causing localized heating that can destroy nearby cancer cells. Likewise, when using magnetic nanoparticles, a high-frequency magnetic field is applied, exciting the fluctuations of the magnetic moment and resulting in magnetic energy release in the form of heat. In other words, it is the use of the photoirradiation of photothermal agents (in this case, NFs) in order to generate heat for the localized thermal damage of solid cancerous tumors [109]. Table 3 presents iron-based nanoflowers synthesized by different processes, and Table 4 shows the synthesized iron nanoflowers under diverse reaction conditions and their main findings.

Table 3. Iron-based nanoflowers synthesized by different processes.

Type of Nanoflower	Synthesis Method	Diameter (nm)	Magnetic Properties	Application	Reference
$Fe_{0.6}Mn_{0.4}O$	One-pot high-temperature thermal decomposition	102.7 ± 11	ferromagnetic	Theranostic agent for MRI and MHT	[110]
Fe_3O_4@PEG	Solvothermal	70–250	superparamagnetic	MRI contrast agent, photothermal agent	[111]
γFe_2O_3@Au	Co-precipitation	179	superparamagnetic	PA and MRI agent, photothermal agent	[112]
γFe_2O_3	Modified polyol	15.1 ± 2.8 35 ± 3.8	superparamagnetic	Cellular imaging MHT agent	[83]
Fe_3O_4@PS-b-PAA	Polyol	49	n.a.	MRI contrast agent, imaging tracer in MPI, photothermal agent	[113]
Fe_2O_3@Au	Polyol	25–30	n.a.	Photothermal agent	[114]
γFe_2O_3@CuS	Polyol	120.4 ± 7.3	superparamagnetic	Theranostic Agent (PTT, PDT, MHT, MRI)	[115]

Table 4. Synthesized iron-based nanoflowers under diverse synthesis parameters and their main findings.

Nanoflower Type	Synthesis Parameters	Main Findings	Ref.
$Fe_{0.6}Mn_{0.4}O$	Temperature: 365 °C; Reaction time: 1 h; Precursors: $Mn(acac)_2$ $Fe(acac)_3$ (0.65:1 mol/mol); Reducing agent/solvent: trioctylamine; Surfactants: oleic acid, oleylamine; Washing solvents: hexane, EtOH.	In imaging: Contrast enhancement in MRI, easier tumor identification. In vitro: Hyperthermia at low dosage against MCF-7 cancer cells. In vivo: Complete tumor inhibition without appreciable side effects on the treated mice.	[110]
Fe_3O_4@PEG	Temperature: 200 °C; Reaction time: 16 h; Precursor: $FeCl_3$ $6H_2O$; Reducing agent: NaAc $3H_2O$; Stabilizer: PEG; Solvent: ethylene glycol; Washing solvents: EtOH, DI H_2O.	In imaging: Magnetic properties for MRI monitoring of the therapeutic process. As a PTT agent: Under 808 nm laser, Fe_3O_4 NFs are more efficient than the reported Fe_3O_4 NPs. In vitro and in vivo results show that they are comparable to black TiO_2@PEG NPs.	[111]

Table 4. *Cont.*

Nanoflower Type	Synthesis Parameters	Main Findings	Ref.
γFe_2O_3@Au	Temperature: 100 °C; Reaction time: 13 h; Precursors: $FeCl_3$ $6H_2O$, $FeCl_2$ $4H_2O$ (2.6:1 *w*/*w*); Precipitating agent: NaOH soln (1.5 M); Oxidizing agent: HNO_3; Solvents: HCl soln (0.4 M); Washing solvent: DI H_2O.	In imaging: Ultrasensitivity to SERS, anatomical localization using PA imaging, spatial resolution from MRI for tumor localization and boundary identification. As a PTT agent: Efficient ablation of tumor under the NIR irradiation without regrowth.	[112]
γFe_2O_3	Temperature: 210 °C; Reaction time: 7.5 h; Precursors: $FeCl_3$ $6H_2O$, $FeCl_2$ $4H_2O$, (2:1 mol/mol); Reducing agents/surfactants/solvents: N-methyldiethanolamine, diethylene glycol; Reduction assistant agent: NaOH; Oxidizing agent: $Fe(NO_3)_3$ $9H_2O$; Washing solvents: EtOH, ethyl acetate, HNO_3 soln (10%), diethyl ether.	In imaging: Could be used in cellular imaging. As a MHT agent: Both NFs' sizes showed a concentration-dependent magnetothermal response. In vitro: There was no hemolysis or notable changes in the morphology of RBCs. All formulations tested in LLC and CULA lung cancer cell lines exhibited minimal effects without magnetic hyperthermia (MHT). However, following exposure to an alternating magnetic field (AMF), cell viability significantly decreased.	[83]
Fe_3O_4@PS-b-PAA	Temperature: 220 °C; Reaction atmosphere: N_2; Reaction time: 1.5 h; Precursor: $FeCl_3$ $6H_2O$, $FeCl_2$ $4H_2O$, (2:1 mol/mol); Reducing agents/surfactants/solvents: N-methyldiethanolamine, diethylene glycol; Reduction assistant agent: NaOH; Solvents: Type 1 H_2O, THF; Solubility enhancing agents: citric acid, oleic acid; Stabilizer: PS-b-PAA; Washing solvents: HNO_3 soln (10%), EtOH, acetone, methanol, ethyl ether.	In imaging: Great potential for both Fe_3O_4 NFs and Fe_3O_4@PS-b-PAA NFs as contrast agents for MRI, with the second one performing exceptionally well as an imaging tracer in MPI. As a PTT agent: Light-to-heat conversion was not affected by the polymer surrounding the NFs. In vivo: Fe_3O_4@PS-b-PAA are biocompatible with the tested glioblastoma cell line.	[113]
Fe_3O_4@Au	Temperature: 220 °C; Reaction time: 5.5 h; Precursors: $FeCl_3$ $6H_2O$, $FeCl_2$ $4H_2O$, (4:1 mol/mol); Reducing agents/surfactants/solvents: N-methyldiethanolamine, diethylene glycol; Reduction assistant agent: NaOH; Oxidizing agent: $Fe(NO_3)_3$ $9H_2O$; Solvent: Type 1 H_2O; Washing solvents: EtOH, ethyl acetate, HNO_3 soln (10%), acetone, diethyl ether.	As a PTT agent: NPs' accumulation in CAFs, resulting in a cumulative effect of PTT treatment. The efficiency of Au-Fe_3O_4 NFs varies based on the injected dose, the irradiation time and the number of laser expositions. Cancer-associated fibroblasts targeted PTT modulates the physical properties of the solid tumors, followed by tumor regression.	[114]
γFe_2O_3@CuS	Temperature: 220 °C; Reaction time: 3.5 h; PrecursorsFeCl$_3$ $6H_2O$, $FeCl_2$ $4H_2O$, (2:1 mol/mol); Reducing agents/surfactants/solvents: N-methyldiethanolamine, diethylene glycol; Reduction assistant agent: NaOH; Washing solvents: EtOH, ethyl acetate, HNO_3 soln (10%), acetone, diethyl ether.	Achievement of a reduced NP-administered dose, reduced laser power exposure and the possibility of serial heating cycles and therapy monitoring by photoacoustic (PA) and magnetic resonance imaging (MRI). Achievement of integration of the dual heating capability (MHT + PTT) with the PDT.	[115]

Liu et al., produced ferromagnetic $Fe_{0.6}Mn_{0.4}O$ NFs and tested their properties. Their results showed that the produced NFs had great potential as a negative and a positive contrast agent in MRI, thus contributing to a more spot-on diagnosis and reducing the chances of the misdiagnosis of other entities as cancerous tumors [110]. Saeed et al., produced PEG-coated Fe_3O_4 NFs through the solvothermal method with easy dimension control for the diagnosis and therapy of breast cancer. Moreover, it was proven that the magnetization of the Fe NFs has a linear relationship with their size, making them excellent for imaging purposes and monitoring therapeutic performance [111].

Therapeutic action against breast cancer cells is also supported by Huang et al. In their study, γFe_2O_3@Au NFs were produced and tested in vivo on mice. It was observed that the produced NPs had a great tumor accumulation and gradual concentration decrease at the 6, 24 and 48 h time stamps post injection. The NF's anticancerous properties were only apparent when applied in combination with laser irradiation. In other cases, in which the separate use of γFe_2O_3@Au NFs or laser irradiation was applied, tumor growth was not influenced. Tumor necrosis was triggered as soon as two days post injection, and no regrowth was observed during the course of 12 days post injection [112].

Furthermore, Theodosiou et al., examined the effect of iron oxide NFs encapsulated in thermosensitive fluorescent liposomes for the hyperthermia treatment of lung adenocarcinoma. In their experiments, NFs managed to easily pass through the lung cancer cells' membranes due to the high biocompatibility provided by the surrounding lipid capsule, therefore accumulating in their cytoplasm. As mentioned before, cytotoxicity showed a negligible effect without a source of radiation, in this case, MHT, thus reinforcing the synergetic effect of NFs [83].

Similarly, iron NFs encapsulated with the polymer PS-PAA have also been examined as multimodal nanoplatforms on one of the most aggressive types of cancer: brain glioblastoma. Benassai et al., developed IONFs@PS-b-PAA for PTT, MRI and magnetic particle imaging (MPI) [113]. Boluda et al., synthesized iron oxide–gold nanoparticles (GIONFs) with great optical properties and biocompatibility and tested them as a PTT agent. In their study, the effect of GIONFs on cholangiocarcinoma (CAA), an aggressive type of cancer affecting the bile duct, was examined. The synergetic use of the produced NFs with NIR laser irradiation resulted in an increase in the tumor's temperature, indicating the high heating capacity of GIONFs. In vitro testing on CAA cells showed that GIONFs do not induce hemolysis. In vivo PTT experiments revealed that a dose of 200 μg GIONFs only reduced the stiffness of the tumor but did not induce its regression. A dose of 700 μg GIONFs showed a partial tumor regression, suggesting that GIONFs should have an auxiliary role in cancer therapeutics [114].

Curcio et al., created iron oxide NFs with an outer Cu_2O shell with multimodal properties including PTT, MHT and PDT. The produced nanomaterials were tested on human prostate adenocarcinoma PC3 cells both in vitro and induced on mice. The in vitro sole use of laser irradiation, magnetic frequencies or nanoparticles showed a negligible effect on PC3 cells. Comparing PTT and MHT, the first showed excellent results, reaching 90% cytotoxicity in 5 min with a concentration of 1.6 mM Cu and 250 μM Fe, while the latter reached only 15% cytotoxicity. It was observed that the effect of NFs in PTT is dose-dependent, even in low concentrations; for example, in 0.16 mM Cu and 25 μM Fe, the NPs showed great results. Taking into consideration that PDT's cytotoxicity depends on oxygen production, IONF@CuSs are eligible for this application due to the production of reactive oxygen species (ROS), especially under laser irradiation. Overall, IONF@CuS provides multiple theranostic applications, especially in PTT [115].

Jing et al., reported that the produced FHCPC@MnO_2 NFs have the ability to be responsive to the TME, typically increasing oxygen levels and decreasing the pH and releasing anticancer drugs, therefore overall contributing to the optimization of therapy. The main advantages of FHCPC@MnO_2 NFs include their simple development through a two-step process, biodegradability, and in vivo fluorescence during MRI scans [116].

4.2. Copper-Based NFs

Copper-based NFs also play an important role in the development of novel theranostic modalities for cancer. Chen et al., synthesized CuS–MnS_2 NFs via a hydrothermal process followed by calcination thermal treatment. Biomedical applications on human ovarian carcinoma A2780 cells, human hepatocyte LO2 cells and MIHA cells, human non-small cell lung cancer H460 cells, and human lung adenocarcinoma A549 cells were examined along with the NFs' anticancer mechanism. Cells were incubated with CuS–MnS_2 NFs and exposed to 808 nm laser irradiation for 15 min along with a fluorescent agent in order to test cell viability. As was expected, higher doses of NFs showed better efficiency. At the highest concentration tested (1 mg mL^{-1}), A2780 cells showed the lowest viability around 65%, H460 70% and A549 around 90%. Compared to cancer cells, healthy human cells MIHA and LO2 were not affected, suggesting that CuS–MnS_2 exhibits good biocompatibility. Further tests were conducted, proving that necroptosis might be the main anticancer mechanism of CuS–MnS_2 NFs paired with NIR irradiation [117]. CuS NFs conjugated with nanographene oxide (NGO) and folic acid (FA) were tested for their efficacy in PTT by Neelgund et al. In their study, the produced NFs showed 46.2% photothermal efficiency (light-to-heat conversion), while only within 5 min of exposure at 980 nm laser irradiation, a temperature of 63.1 °C was accomplished. Notable cytotoxicity was exhibited towards human cervix adenocarcinoma and human ovarian adenocarcinoma cells [118]. Table 5 presents copper-based nanoflowers synthesized by different processes, and Table 6 presents the synthesized copper nanoflowers under diverse reaction conditions and their main findings.

Table 5. Copper-based nanoflowers synthesized by different processes.

Type of Nanoflower	Synthesis Method	Size (nm)	Application	Reference
CuS–MnS_2	Hydrothermal	400	Contrast agent (MRI), photothermal (PTT) and photodynamic (PDT) agent against ovarian cancer	[117]
NGO–FA–CuS	Hydrothermal	40	Theranostic agent	[118]
Cu-EGCG-ICG-DOX	Self-assembly	217 ± 18.1	PTT and chemotherapy agent	[119]
$Cu_{7.2}S_4$/5MoS_2	Solvothermal	200	Theranostic agent (PTT, PDT, CT)	[120]
Hollow CuS	Laser-assisted ablation/ion-exchange	30–120	Theranostic agent (MRI, PTT, DOX-mediated chemotherapy)	
Cu_3SnS_4	Hydrothermal	n.a.	Photoelectrochemical (PEC) detection of human cytochrome c	[121]
$CaMoO_4$/MoS_2/CuS	Hydrothermal	~1000	Enzyme-like action for cancer cell detection and ROS-mediated treatment	[23]
Gallic acid–Cu(II)	Self-assembly	9200	Anticancer activity against breast and lung cancer cell lines	[122]

Table 6. Synthesized copper-based nanoflowers under diverse reaction conditions and their main findings.

Nanoflower Type	Reaction Parameters	Main Findings	Ref.
$CuS–MnS_2$	Temperature: 100 °C Reaction time: 4 h Precursors: Thioacetamide, $CuCl_2.2H_2O$, $MnCl_2$ $4H_2O$, (15:5:1 mol/mol/mol); Surfactant: sodium dodecylbenzensulphonate; Solvent: H_2O; Washing solvents: EtOH, H_2O.	Potential use as theranostic agents for MRI and PDT/PTT for cancer. Necroptosis might be their main anticancer mechanism of action.	
NGO–FA–CuS	Temperature: 150 °C Reaction time: 6 h Precursors: $Cu(NO_3)_2$; Reducing agent: thioglycolic acid; Solvent: Type 1 H_2O; Washing solvents: EtOH, DI H_2O; Other materials: Folic acid-conjugated nanographene oxide.	Multifunctional photothermal agent that causes nuclear targeting, accumulation and necrosis of cancer cells by hypothermia.	[118]
Cu-EGCG-ICG-DOX	Temperature: room temperature; Reaction time: 4.5 h; Precursor: $CuCl_2$; Solvent: triethanolamine. Drugs: (−)-epigallocatechin-3-gallate, indocyanine green, doxorubicin hydrochloride.	Long-term drug retention in tumor above 8 d. Upon NIR laser irradiation, high NIR-II fluorescence signals could image guide local PTT-chemotherapy of tumors and suppress tumor growth until 14 d.	[119]
$Cu_{7.2}S_4/5MoS_2$	Temperature: 200 °C; Reaction time: 24 h; Precursors: $(NH_4)_2MoO_4$, $Cu(CO_2CH_3)_2$, thioacetamide, (0.58:1.2:2.3 mol/mol/mol); Solvents: Type 1 H_2O, PEG-400; Washing solvents: EtOH, Type 1 H_2O.	Both in vivo and in vitro: Synergetic therapeutic effect between PTT, CDT, PDT in vivo: photoacoustic signal amplitudes and computed tomographic contrast enhancement.	[120]
hollow CuS	Temperature: 60 °C; Reaction time: 2 h; Precursor: $Cu(NO_3)_2$ $3H_2O$; Solvent: Type 1 H_2O; Washing solvents: Type 1 H_2O; Other materials: ZnO nanoparticles.	Effective theranostic agent for MRI-guided synergetic thermochemotherapy. Exhibits (a) 1.6 times larger longitudinal mass relaxation rate than that of the T_1 MRI contrast agent Magnevist and (b) photothermal conversion efficiency of 30%.	[123]
Cu_3SnS_4	Temperature: 200 °C; Reaction time: 3 h; Precursors $SnCl_4$ $5H_2O$, $CuCl_2$, thioacetamide (13.3:4.4); Stabilizer: EDTA; Reducing agent: NaOH; Solvent: DI H_2O; Washing solvents: DI H_2O, anhydrous EtOH;	PEC immunosensor detects human serum Cyt *c* at concentrations of 1 fM-1000 nM (limit of detection: 0.35 fM).	[121]
$CaMoO_4/MoS_2/CuS$	Temperature: 180 °C; Reaction time: 6 h; Precursor: $CaCl_2$, Na_2MoO_4 $2H_2O$, thiourea, $Cu(NO_3)_2$ $2H_2O$ (6:2.5:13:3); Stabilizer: PVP; Reducing agent: citric acid; Solvent: dH_2O; Washing solvents: absolute EtOH, dH_2O.	Provides MDA-MB-231 cell detection at concentrations of 50–5.5 × 10^4 cells/mL (limit of detection: 10 cells/mL). By generating reactive oxygen species, cancer cells were treated.	[23]
Gallic acid–Cu(II)	Temperature: room temperature; Reaction time: 72 h; Precursor: $CuSO_4$ $5H_2O$, gallic acid; Solvent: UP H_2O, PBS.	Cytotoxic effects against MCF7 and A549 cancer cell lines, showing apoptotic cell death percentages of 67% and 65%, respectively.	[122]

Liao et al., synthesized self-assembled Cu HNFs loaded with epigallocatechin-3-gallate (EGCG), indocyanine green (ICG) and doxorubicin hydrochloride (DOX) (referred to as ICG ⊃ EDOX), based on the metal coordination effect, hydrophobic interactions and π-π stacking between the reagents. EGCG was used for its biocompatibility, ICG works as an excellent photoabsorbing agent causing green fluorescence, and DOX is a common drug used against cancer. After the characterization of the nanomaterial, it was found that DOX made up 42.1 wt%, indicating high drug load efficiency. The produced HNFs exhibited responsive behavior to acidic pH (a characteristic of TME), releasing ICG ⊃ DOX at a rate of 13.5% at a pH = 7.4 and 33.1% at a pH = 5 (both measurements were conducted 108 h post injection). The synergetic effect between the HNFs and PTT became obvious when NIR laser irradiation was applied at a pH = 5, and the release percentage of ICG ⊃ DOX increased up to 60.8%. The in vitro cytotoxicity of HNFs was tested on murine mammary carcinoma (4T1) cells. The most efficient method proved to be ICG ⊃ DOX combined with laser irradiation, as the viability of 4T1 cells was valued at 47.9%. Moreover, no hemolysis of red blood cells was observed after they were being treated with ICG ⊃ EDOX. Concerning in vivo experiments, it was noted that mice with administrated ICG ⊃ EDOX did not exhibit hair loss, weight loss and tissues damages so severely compared to mice who were only administrated DOX.

Wu et al., synthesized PEG $Cu_{7.2}S_4/5MoS_2$ composite NFs (CSMS-PEG CNFs) in a one-pot approach, using the solvothermal method. The in vitro cytotoxicity of CSMS-PEG CNFs was examined on 4T1 cells. The sole use of NFs did not influence the cells' viability, whereas the highest concentration of NFs (200 μg mL^{-1}), combined with laser irradiation, imposed death on 78% of tumor cells. The photothermic conversion of CSMS-PEG CNFs was tested in different concentrations. It was proved that under a laser irradiation of 808 nm, the sample with 200 μg mL^{-1} showed the highest PT properties to be 20.9 °C in 500 s, therefore proving a dose-dependent correlation. Moreover, in vivo experiments on mice showed that CSMS-PEG CNFs combined with laser irradiation have a great therapeutic effect on 4T1 cells without a reoccurrence of the tumor [120].

Zhang et al., synthesized CuS NFs and tested them as a multimodal nanomaterial. Firstly, its ability as a nanocarrier of DOX was investigated. Due to its high surface area, the nanomaterial showed a high drug loading capacity as well as time- and pH-dependent behavior in vivo. The amount of DOX released from loaded CuS NFs was at 80.2% at a pH of 4.5, similar to a tumor's microenvironment. Cell viability tests on human hepatocellular carcinoma (HepG2) showed that the synergetic action of CuS-DOX NFs and laser irradiation caused 96.8% cytotoxicity [123].

4.3. Other Applications

Iron- and copper-based NFs have plenty of applications both within and out of the realm of medicine. Firstly, NFs show great antibacterial properties with low values of minimum inhibitory concentration (MIC) comparable to other widely used antibiotics. Eskikaya et al., synthesized NF@FeO(OH) and studied its effect against certain bacterial strands. Their results showed that the MIC was equal to 256 mg L^{-1} for *E. coli*, *C. parapisilosis* and *P. aeruginosa* and 128 mg L^{-1} for *L. pneumophila*, *E. hirae*, and *S. aureus*, and *C. tropicalis*. Its antimicrobial mechanism is probably linked to the changes in microbial DNA and proteins caused by ferric ions [124].

Yilmaz used a green self-assembly method to synthesize hybrid gallic acid–Cu(II) NFs and studied their antimicrobial activity against fungus (*C. albicans*) and Gram-negative (*E. coli*, *P. aeruginosa*) and Gram-positive (*S. aureus*) bacteria. It was found that the hNFs depicted high antimicrobial efficacy at all examined microorganism concentrations [122].

Ingle and Rai synthesized Cu NFs and evaluated their antifungal properties against common plant pathogenic fungi, namely *F. oxysporum*, *F. moniliforme*, *F. culmorum*, *F. tricinctum* and *A. niger*. It was concluded that Cu NFs enhance the action of the commercial antifungal agent ketoconazole despite the NFs' dependence on multiple factors such as

temperature, the concentration of nanoparticles, pH and the concentration of the test organism [125].

5. Limitations and Future Perspectives

The mechanisms underlying the interactions between biomolecules and metal ions are not yet fully understood. Various metal ions can affect the activity of proteins or enzymes involved in the formation of protein–inorganic HNFs; for instance, copper ions may inhibit β-Galactosidase (β-Gal) enzyme activity while enhancing horseradish peroxidase (HRP) enzyme activity. Gaining a deeper insight into these interactions could facilitate the development of protein–inorganic HNFs with optimal biological activity. Additionally, the properties of HNFs, such as morphology and size, significantly influence their performance. Studies suggest that the morphology of organic–inorganic nanohybrids can impact enzymatic activity, with NFs that have a higher surface-to-volume ratio experiencing fewer mass transfer limitations and thus increasing the likelihood of substrate interaction. The size of HNFs is also critical for their performance in various applications; producing nanoflowers with a narrow size distribution is essential for nanoflower-based immunosensors, as size variability can reduce analysis accuracy [35].

Although NFs show a great variety of applications, currently, there is not a fulfilling number of studies or clinical trials investigating their impact towards living organisms or the environment and/or the ecological balance.

Also, ever since the invention of nanomaterials, nanotoxicity has been a rising concern in the scientific community [126,127]. According to research, NFs tend to be recognized as foreign substances in the body and concentrate in the liver and the spleen [111,116]. Although NFs are non-hemolytic, partial deformations of red blood cell (RBC) morphology is possible [83].

Another limitation of NFs that should be taken into consideration is their variable effect as a therapy modality. According to the literature, the anticancerous action of NFs is not universal to all types of cancer. The viability of cancer cells can vary; for example, breast cancer cells have shown a viability of around 20% [111,112] and 50–70% [110] in different studies, while lung adenocarcinoma cells survived at 70–80% [83]. At the same time, aggressive types of cancer, such as brain glioblastoma, showed 75% viability, even after a high concentration of Fe NFs was applied [113]. On the contrary, NFs acting as a contrast agent in imaging modalities for cancer diagnosis show excellent potential. The future utilization of NFs as a contrast agent could be applied for the diagnosis of other diseases. More specifically, these NPs could especially be useful for the diagnosis of the "silent" diseases, such as atherosclerosis [128], as there is a need for urgent treatment. Further research is imperative for NFs if they are to be used as the main modality in cancer theranostics.

6. Conclusions

Cancer is currently one of the main causes of death internationally. Its complex nature has been gradually revealed, while many imaging and therapeutic modalities have been developed. Advanced modalities in cancer theranostics with a low price range and high yield efficiency are pressing issues. A novel type of materials, nanomaterials like NPs, is being studied as a plausible solution to this problem. NFs are NPs that resemble flowers on the nanoscale. Although a typical NF's structure consists of inorganic materials, many organic components can be added to enhance their properties, such as enzymes and drugs, thus creating HNFs.

The field of flower-like hierarchical nanomaterials has seen significant advancements, focusing on synthetic techniques, growth mechanisms, particle size distribution, morphology, and their chemical, physical, and optical properties to enhance catalytic, energy-related, and biomedical applications. Various inorganic nanoflowers have been synthesized through physical, chemical, biological, and hybrid methods. Over the past two decades, research on these materials has surged, with increasing publications emphasizing their benefits, such

as their high surface-to-volume ratio, strong adsorption capacity, high loading efficiency, and excellent catalytic performance. Efforts have been made to optimize their morphology and size distribution for specific applications by controlling factors like reagents, reaction time, temperature, and metal ratios.

In the last couple of decades, NFs based on copper or iron have been under the microscope for the production of novel nanomaterials. Due to their excellent biocompatibility, high drug loading ability, low cost, facile synthesis and, most importantly, magnetic and photothermic properties, Fe- and Cu-based NFs can be used as drug nanoplatforms, PTT/MHT/PDT agents and MRI contrast agents. NFs have been synthesized through various methods, including physical, chemical, biological, and hybrid approaches. The optimization of their morphology and size distribution is of great importance for specific applications, by adjusting, for example, reaction conditions such as reagent type and quantity, reaction time, temperature, and metal ratios. By altering synthetic pathways, simple, cost-effective, and environmentally friendly methods have been developed that seem to be suitable for industrial applications too. Such NFs possess unique functionalities and hold promise for use in cancer theranostics. Investigations into alloy, core–shell, and surface-modified NFs are anticipated to expand the range of multi-metallic compositions with modified structures, and future research may focus on integrating multiple nanostructured materials. These studies have uncovered numerous unique functionalities and potential applications. Future research on nanomaterials is likely to involve combining multiple nanostructured materials, such as CoS nanoflowers coated with gallic acid, manganese sulfide, and graphene oxides, to unlock new functionalities and expand their applications.

Author Contributions: Conceptualization, A.T. and G.Z.K.; methodology, all authors; software, all authors; validation, A.T. and G.Z.K.; investigation, all authors; data curation, A.V.; writing—original draft preparation, A.V., D.A.G. and P.E.; writing—review and editing, A.T. and G.Z.K.; visualization, A.T. and G.Z.K.; supervision, A.T.; project administration, A.T. and G.Z.K. All authors have read and agreed to the published version of the manuscript.

Funding: This research received no external funding.

Conflicts of Interest: The authors declare no conflicts of interest.

References

1. Siegel, R.L.; Miller, K.D.; Fuchs, H.E.; Jemal, A. Cancer Statistics, 2021. *CA A Cancer J Clin.* **2021**, *71*, 7–33. [CrossRef] [PubMed]
2. Sri, S.; Chauhan, D.; Lakshmi, G.B.V.S.; Thakar, A.; Solanki, P.R. MoS2 Nanoflower Based Electrochemical Biosensor for TNF Alpha Detection in Cancer Patients. *Electrochim. Acta* **2022**, *405*, 139736. [CrossRef]
3. Yarana, C.; St. Clair, D. Chemotherapy-Induced Tissue Injury: An Insight into the Role of Extracellular Vesicles-Mediated Oxidative Stress Responses. *Antioxidants* **2017**, *6*, 75. [CrossRef] [PubMed]
4. Tsoupras, A.; Adamantidi, T.; Finos, M.A.; Philippopoulos, A.; Detopoulou, P.; Tsopoki, I.; Kynatidou, M.; Demopoulos, C.A. Re-Assessing the Role of Platelet Activating Factor and Its Inflammatory Signaling and Inhibitors in Cancer and Anti-Cancer Strategies. *Front. Biosci. (Landmark Ed.)* **2024**, *29*, 345. [CrossRef] [PubMed]
5. Zhang, S.; Li, Q.; Yang, N.; Shi, Y.; Ge, W.; Wang, W.; Huang, W.; Song, X.; Dong, X. Phase-Change Materials Based Nanoparticles for Controlled Hypoxia Modulation and Enhanced Phototherapy. *Adv. Funct. Mater.* **2019**, *29*, 1906805. [CrossRef]
6. Gkika, D.A.; Tolkou, A.K.; Evgenidou, E.; Bikiaris, D.N.; Lambropoulou, D.A.; Mitropoulos, A.C.; Kalavrouziotis, I.K.; Kyzas, G.Z. Fate and Removal of Microplastics from Industrial Wastewaters. *Sustainability* **2023**, *15*, 6969. [CrossRef]
7. Freire, J.J.; Efthymiopoulos, P.; Ahmadi, A. Simulation Study of the G=4 PAMAM Dendrimer in Water at Different pH Conditions. *Per. Politech. Chem. Eng.* **2014**, *58*, 49. [CrossRef]
8. Zhang, S.; Cao, C.; Lv, X.; Dai, H.; Zhong, Z.; Liang, C.; Wang, W.; Huang, W.; Song, X.; Dong, X. A H_2O_2 Self-Sufficient Nanoplatform with Domino Effects for Thermal-Responsive Enhanced Chemodynamic Therapy. *Chem. Sci.* **2020**, *11*, 1926–1934. [CrossRef]
9. Chen, D.; Tang, Q.; Zou, J.; Yang, X.; Huang, W.; Zhang, Q.; Shao, J.; Dong, X. pH-Responsive PEG–Doxorubicin-Encapsulated Aza-BODIPY Nanotheranostic Agent for Imaging-Guided Synergistic Cancer Therapy. *Adv. Healthc. Mater.* **2018**, *7*, 1701272. [CrossRef]
10. Sheikh Mohamed, M.; Veeranarayanan, S.; Maekawa, T.; Sakthi Kumar, D. External Stimulus Responsive Inorganic Nanomaterials for Cancer Theranostics. *Adv. Drug Deliv. Rev.* **2019**, *138*, 18–40. [CrossRef]
11. Yan, S.; Zhang, G.; Luo, W.; Xu, M.; Peng, R.; Du, Z.; Liu, Y.; Bai, Z.; Xiao, X.; Qin, S. PROTAC Technology: From Drug Development to Probe Technology for Target Deconvolution. *Eur. J. Med. Chem.* **2024**, *276*, 116725. [CrossRef] [PubMed]

12. Liu, H.; Chen, W.; Wu, G.; Zhou, J.; Liu, C.; Tang, Z.; Huang, X.; Gao, J.; Xiao, Y.; Kong, N.; et al. Glutathione-Scavenging Nanoparticle-Mediated PROTACs Delivery for Targeted Protein Degradation and Amplified Antitumor Effects. *Adv. Sci.* **2023**, *10*, 2207439. [CrossRef] [PubMed]
13. Fang, T.; Duarte, J.N.; Ling, J.; Li, Z.; Guzman, J.S.; Ploegh, H.L. Structurally Defined αMHC-II Nanobody–Drug Conjugates: A Therapeutic and Imaging System for B-Cell Lymphoma. *Angew. Chem. Int. Ed.* **2016**, *55*, 2416–2420. [CrossRef] [PubMed]
14. Lewińska, A.; Radoń, A.; Gil, K.; Błoniarz, D.; Ciuraszkiewicz, A.; Kubacki, J.; Kądziołka-Gaweł, M.; Łukowiec, D.; Gębara, P.; Krogul-Sobczak, A.; et al. Carbon-Coated Iron Oxide Nanoparticles Promote Reductive Stress-Mediated Cytotoxic Autophagy in Drug-Induced Senescent Breast Cancer Cells. *ACS Appl. Mater. Interfaces* **2024**, *16*, 15457–15478. [CrossRef]
15. Barani, M.; Bilal, M.; Sabir, F.; Rahdar, A.; Kyzas, G.Z. Nanotechnology in Ovarian Cancer: Diagnosis and Treatment. *Life Sci.* **2021**, *266*, 118914. [CrossRef]
16. Kashyap, B.K.; Singh, V.V.; Solanki, M.K.; Kumar, A.; Ruokolainen, J.; Kesari, K.K. Smart Nanomaterials in Cancer Theranostics: Challenges and Opportunities. *ACS Omega* **2023**, *8*, 14290–14320. [CrossRef]
17. Losada-Garcia, N.; Vazquez-Calvo, A.; Ortega-Alarcon, D.; Abian, O.; Velazquez-Campoy, A.; Domingo-Calap, P.; Alcami, A.; Palomo, J.M. Nanostructured Biohybrid Material with Wide-Ranging Antiviral Action. *Nano Res.* **2023**, *16*, 11455–11463. [CrossRef]
18. Losada-Garcia, N.; Vazquez-Calvo, A.; Alcami, A.; Palomo, J.M. Preparation of Highly Stable and Cost-Efficient Antiviral Materials for Reducing Infections and Avoiding the Transmission of Viruses Such as SARS-CoV-2. *ACS Appl. Mater. Interfaces* **2023**, *15*, 22580–22589. [CrossRef]
19. Hachani, R.; Lowdell, M.; Birchall, M.; Hervault, A.; Mertz, D.; Begin-Colin, S.; Thanh, N.T.K. Polyol Synthesis, Functionalisation, and Biocompatibility Studies of Superparamagnetic Iron Oxide Nanoparticles as Potential MRI Contrast Agents. *Nanoscale* **2016**, *8*, 3278–3287. [CrossRef]
20. Bao, Y.; Sherwood, J.A.; Sun, Z. Magnetic Iron Oxide Nanoparticles as T_1 Contrast Agents for Magnetic Resonance Imaging. *J. Mater. Chem. C* **2018**, *6*, 1280–1290. [CrossRef]
21. Vodyashkin, A.; Stoinova, A.; Kezimana, P. Promising Biomedical Systems Based on Copper Nanoparticles: Synthesis, Characterization, and Applications. *Colloids Surf. B Biointerfaces* **2024**, *237*, 113861. [CrossRef] [PubMed]
22. Storozhuk, L.; Besenhard, M.O.; Mourdikoudis, S.; LaGrow, A.P.; Lees, M.R.; Tung, L.D.; Gavriilidis, A.; Thanh, N.T.K. Stable Iron Oxide Nanoflowers with Exceptional Magnetic Heating Efficiency: Simple and Fast Polyol Synthesis. *ACS Appl. Mater. Interfaces* **2021**, *13*, 45870–45880. [CrossRef] [PubMed]
23. Murugan, C.; Lee, H.; Park, S. A Self-Assembled Three-Dimensional Hierarchical Nanoflower: An Efficient Enzyme-Mimetic Material for Cancer Cell Detection That Improves ROS Generation for Therapy. *Nanoscale Adv.* **2024**, *6*, 590–605. [CrossRef] [PubMed]
24. Naz, S.; Gul, A.; Zia, M.; Javed, R. Synthesis, Biomedical Applications, and Toxicity of CuO Nanoparticles. *Appl. Microbiol. Biotechnol.* **2023**, *107*, 1039–1061. [CrossRef] [PubMed]
25. Dang, W.; Li, T.; Li, B.; Ma, H.; Zhai, D.; Wang, X.; Chang, J.; Xiao, Y.; Wang, J.; Wu, C. A Bifunctional Scaffold with $CuFeSe_2$ Nanocrystals for Tumor Therapy and Bone Reconstruction. *Biomaterials* **2018**, *160*, 92–106. [CrossRef]
26. Pastrián, F.A.C.; Da Silva, A.G.M.; Dourado, A.H.B.; De Lima Batista, A.P.; De Oliveira-Filho, A.G.S.; Quiroz, J.; De Oliveira, D.C.; Camargo, P.H.C.; Córdoba De Torresi, S.I. Why Could the Nature of Surface Facets Lead to Differences in the Activity and Stability of Cu_2O-Based Electrocatalytic Sensors? *ACS Catal.* **2018**, *8*, 6265–6272. [CrossRef]
27. Geonmonond, R.S.; Silva, A.G.M.D.; Camargo, P.H.C. Controlled Synthesis of Noble Metal Nanomaterials: Motivation, Principles, and Opportunities in Nanocatalysis. *An. Acad. Bras. Ciênc.* **2018**, *90*, 719–744. [CrossRef]
28. Shende, P.; Kasture, P.; Gaud, R.S. Nanoflowers: The Future Trend of Nanotechnology for Multi-Applications. *Artif. Cells Nanomed. Biotechnol.* **2018**, *46*, 413–422. [CrossRef]
29. Zeng, J.; Xia, Y. Not Just a Pretty Flower. *Nat. Nanotech.* **2012**, *7*, 415–416. [CrossRef]
30. Khakbiz, M.; Shakibania, S.; Ghazanfari, L.; Zhao, S.; Tavakoli, M.; Chen, Z. Engineered Nanoflowers, Nanotrees, Nanostars, Nanodendrites, and Nanoleaves for Biomedical Applications. *Nanotechnol. Rev.* **2023**, *12*, 20220523. [CrossRef]
31. Ge, J.; Lei, J.; Zare, R.N. Protein–Inorganic Hybrid Nanoflowers. *Nat. Nanotechnol.* **2012**, *7*, 428–432. [CrossRef] [PubMed]
32. Mazumder, J.A.; Ahmad, A.; Ali, J.; Noori, R.; Bhuyan, T.; Sardar, M.; Sheehan, D. Biomimetic Green Synthesis of ZnO Nanoflowers Using α-Amylase: From Antimicrobial to Toxicological Evaluation. *Sci. Rep.* **2024**, *14*, 16566. [CrossRef] [PubMed]
33. Chormey, D.S.; Erarpat, S.; Zaman, B.T.; Özdoğan, N.; Yağmuroğlu, O.; Bakırdere, S. Nanoflower Synthesis, Characterization and Analytical Applications: A Review. *Environ. Chem. Lett.* **2023**, *21*, 1863–1880. [CrossRef]
34. Abid, N.; Khan, A.M.; Shujait, S.; Chaudhary, K.; Ikram, M.; Imran, M.; Haider, J.; Khan, M.; Khan, Q.; Maqbool, M. Synthesis of Nanomaterials Using Various Top-down and Bottom-up Approaches, Influencing Factors, Advantages, and Disadvantages: A Review. *Adv. Colloid Interface Sci.* **2022**, *300*, 102597. [CrossRef]
35. Liu, Y.; Ji, X.; He, Z. Organic–Inorganic Nanoflowers: From Design Strategy to Biomedical Applications. *Nanoscale* **2019**, *11*, 17179–17194. [CrossRef]
36. Lee, S.J.; Jang, H.; Lee, D.N. Inorganic Nanoflowers—Synthetic Strategies and Physicochemical Properties for Biomedical Applications: A Review. *Pharmaceutics* **2022**, *14*, 1887. [CrossRef]
37. Liu, Y.; Wang, B.; Ji, X.; He, Z. Self-Assembled Protein-Enzyme Nanoflower-Based Fluorescent Sensing for Protein Biomarker. *Anal. Bioanal. Chem.* **2018**, *410*, 7591–7598. [CrossRef]

38. Pormohammad, A.; Turner, R.J. Silver Antibacterial Synergism Activities with Eight Other Metal(Loid)-Based Antimicrobials against Escherichia Coli, Pseudomonas Aeruginosa, and Staphylococcus Aureus. *Antibiotics* **2020**, *9*, 853. [CrossRef]
39. Meister, T.L.; Fortmann, J.; Breisch, M.; Sengstock, C.; Steinmann, E.; Köller, M.; Pfaender, S.; Ludwig, A. Nanoscale Copper and Silver Thin Film Systems Display Differences in Antiviral and Antibacterial Properties. *Sci. Rep.* **2022**, *12*, 7193. [CrossRef]
40. Hao, Z.; Wang, M.; Cheng, L.; Si, M.; Feng, Z.; Feng, Z. Synergistic Antibacterial Mechanism of Silver-Copper Bimetallic Nanoparticles. *Front. Bioeng. Biotechnol.* **2024**, *11*, 1337543. [CrossRef]
41. Kulkarni, S.K. *Nanotechnology: Principles and Practices*; Springer International Publishing: Cham, Switzerland, 2015; ISBN 978-3-319-09170-9.
42. Kritika; Roy, I. Therapeutic Applications of Magnetic Nanoparticles: Recent Advances. *Mater. Adv.* **2022**, *3*, 7425–7444. [CrossRef]
43. Marciello, M.; Luengo, Y.; Morales, M.P. *Iron Oxide Nanoparticles for Cancer Diagnosis and Therapy*; Elsevier: Amsterdam, The Netherlands, 2016; pp. 667–694.
44. Lee, S.Y.; Tan, Y.H.; Lau, S.Y.; Mubarak, N.M.; Tan, Y.Y.; Tan, I.S.; Lee, Y.H.; Ibrahim, M.L.; Karri, R.R.; Khalid, M.; et al. A State-of-the-Art Review of Metal Oxide Nanoflowers for Wastewater Treatment: Dye Removal. *Environ. Res.* **2024**, *259*, 119448. [CrossRef] [PubMed]
45. Bokov, D.; Turki Jalil, A.; Chupradit, S.; Suksatan, W.; Javed Ansari, M.; Shewael, I.H.; Valiev, G.H.; Kianfar, E. Nanomaterial by Sol-Gel Method: Synthesis and Application. *Adv. Mater. Sci. Eng.* **2021**, *2021*, 5102014. [CrossRef]
46. Mahato, S.S.; Mahata, D.; Panda, S.; Mahata, S.; Mahato, S.S.; Mahata, D.; Panda, S.; Mahata, S. Perspective Chapter: Sol-Gel Science and Technology in Context of Nanomaterials—Recent Advances. In *Sol-Gel Method—Recent Advances*; IntechOpen: London, UK, 2023; ISBN 978-1-80355-415-0.
47. Parashar, M.; Shukla, V.K.; Singh, R. Metal Oxides Nanoparticles via Sol–Gel Method: A Review on Synthesis, Characterization and Applications. *J. Mater. Sci. Mater. Electron.* **2020**, *31*, 3729–3749. [CrossRef]
48. Chen, P.; Zhang, P.; Cui, Y.; Fu, X.; Wang, Y. Recent Progress in Copper-Based Inorganic Nanostructure Photocatalysts: Properties, Synthesis and Photocatalysis Applications. *Mater. Today Sustain.* **2023**, *21*, 100276. [CrossRef]
49. Modan, E.M.; Plăiașu, A. Advantages and Disadvantages of Chemical Methods in the Elaboration of Nanomaterials. *Ann. Dunarea Jos Univ. Galati Fascicle IX Metall. Mater. Sci.* **2020**, *43*, 53–60. [CrossRef]
50. Continuous Hydrothermal Synthesis of Inorganic Nanoparticles: Applications and Future Directions | Chemical Reviews. Available online: https://pubs.acs.org/doi/full/10.1021/acs.chemrev.6b00417 (accessed on 18 October 2024).
51. Banoth, P.; Sohan, A.; Kandula, C.; Kanaka, R.K.; Kollu, P. Microwave-Assisted Solvothermal Route for One-Step Synthesis of Pure Phase Bismuth Ferrite Microflowers with Improved Magnetic and Dielectric Properties. *ACS Omega* **2022**, *7*, 12910–12921. [CrossRef]
52. Zhou, Y.; Zeng, B.; Zhou, R.; Li, X.; Zhang, G. One-Pot Synthesis of Multiple Stimuli-Responsive Magnetic Nanomaterials Based on the Biomineralization of Elastin-like Polypeptides. *ACS Omega* **2021**, *6*, 27946–27954. [CrossRef]
53. Vigil, T.N.; Spangler, L.C. Understanding Biomineralization Mechanisms to Produce Size-Controlled, Tailored Nanocrystals for Optoelectronic and Catalytic Applications: A Review. *ACS Appl. Nano Mater.* **2024**, *7*, 18626–18654. [CrossRef]
54. Głowniak, S.; Szczęśniak, B.; Choma, J.; Jaroniec, M. Recent Developments in Sonochemical Synthesis of Nanoporous Materials. *Molecules* **2023**, *28*, 2639. [CrossRef]
55. Alonso-Lemus, I.L.; Figueroa-Torres, M.Z.; García-Hernández, A.B.; Escobar-Morales, B.; Rodríguez-Varela, F.J.; Fuentes, A.F.; Lardizabal-Gutierrez, D.; Quintana-Owen, P. Low-Cost Sonochemical Synthesis of Nitrogen-Doped Graphene Metal-Free Electrocatalyst for the Oxygen Reduction Reaction in Alkaline Media. *Int. J. Hydrogen Energy* **2017**, *42*, 30330–30338. [CrossRef]
56. Fiévet, F.; Ammar-Merah, S.; Brayner, R.; Chau, F.; Giraud, M.; Mammeri, F.; Peron, J.; Piquemal, J.-Y.; Sicard, L.; Viau, G. The Polyol Process: A Unique Method for Easy Access to Metal Nanoparticles with Tailored Sizes, Shapes and Compositions. *Chem. Soc. Rev.* **2018**, *47*, 5187–5233. [CrossRef] [PubMed]
57. Baričić, M.; Nuñez, J.M.; Aguirre, M.H.; Hrabovsky, D.; Seydou, M.; Meneghini, C.; Peddis, D.; Ammar, S. Advancements in Polyol Synthesis: Expanding Chemical Horizons and Néel Temperature Tuning of CoO Nanoparticles. *Sci. Rep.* **2024**, *14*, 12529. [CrossRef] [PubMed]
58. Dong, H.; Chen, Y.-C.; Feldmann, C. Polyol Synthesis of Nanoparticles: Status and Options Regarding Metals, Oxides, Chalcogenides, and Non-Metal Elements. *Green Chem.* **2015**, *17*, 4107–4132. [CrossRef]
59. Lee, S.J.; Jang, H.; Lee, D.N. Recent Advances in Nanoflowers: Compositional and Structural Diversification for Potential Applications. *Nanoscale Adv.* **2023**, *5*, 5165–5213. [CrossRef] [PubMed]
60. Adeola, A.O.; Duarte, M.P.; Naccache, R. Microwave-Assisted Synthesis of Carbon-Based Nanomaterials from Biobased Resources for Water Treatment Applications: Emerging Trends and Prospects. *Front. Carbon* **2023**, *2*, 1220021. [CrossRef]
61. Kustov, L.; Vikanova, K. Synthesis of Metal Nanoparticles under Microwave Irradiation: Get Much with Less Energy. *Metals* **2023**, *13*, 1714. [CrossRef]
62. Mohammadi, H.; Nekobahr, E.; Akhtari, J.; Saeedi, M.; Akbari, J.; Fathi, F. Synthesis and Characterization of Magnetite Nanoparticles by Co-Precipitation Method Coated with Biocompatible Compounds and Evaluation of in-Vitro Cytotoxicity. *Toxicol. Rep.* **2021**, *8*, 331–336. [CrossRef]
63. Kandasamy, G.; Sudame, A.; Luthra, T.; Saini, K.; Maity, D. Functionalized Hydrophilic Superparamagnetic Iron Oxide Nanoparticles for Magnetic Fluid Hyperthermia Application in Liver Cancer Treatment. *ACS Omega* **2018**, *3*, 3991–4005. [CrossRef]

64. Shahri, Z.; Salavati-Niasari, M.; Mir, N.; Kianpour, G. Facile Synthesis and Characterization of Nanostructured Flower-like Copper Molybdate by the Co-Precipitation Method. *J. Cryst. Growth* **2014**, *386*, 80–87. [CrossRef]
65. Dayan, S.; Altinkaynak, C.; Kayaci, N.; Doğan, Ş.D.; Özdemir, N.; Ozpozan, N.K. Hybrid Nanoflowers Bearing Tetraphenylporphyrin Assembled on Copper(II) or Cobalt(II) Inorganic Material: A Green Efficient Catalyst for Hydrogenation of Nitrobenzenes in Water. *Appl. Organomet. Chem.* **2020**, *34*, e5381. [CrossRef]
66. El-Khawaga, A.M.; Zidan, A.; El-Mageed, A.I.A.A. Preparation Methods of Different Nanomaterials for Various Potential Applications: A Review. *J. Mol. Struct.* **2023**, *1281*, 135148. [CrossRef]
67. Rane, A.V.; Kanny, K.; Abitha, V.K.; Thomas, S. Methods for Synthesis of Nanoparticles and Fabrication of Nanocomposites. In *Synthesis of Inorganic Nanomaterials*; Elsevier: Amsterdam, The Netherlands, 2018; pp. 121–139; ISBN 978-0-08-101975-7.
68. Möller, M.; Harnisch, F.; Schröder, U. Microwave-Assisted Hydrothermal Degradation of Fructose and Glucose in Subcritical Water. *Biomass Bioenergy* **2012**, *39*, 389–398. [CrossRef]
69. Tzanetis, K.F.; Posada, J.A.; Ramirez, A. Analysis of Biomass Hydrothermal Liquefaction and Biocrude-Oil Upgrading for Renewable Jet Fuel Production: The Impact of Reaction Conditions on Production Costs and GHG Emissions Performance. *Renew. Energy* **2017**, *113*, 1388–1398. [CrossRef]
70. Yang, G.; Park, S.-J. Conventional and Microwave Hydrothermal Synthesis and Application of Functional Materials: A Review. *Materials* **2019**, *12*, 1177. [CrossRef]
71. Cheah, P.; Qu, J.; Li, Y.; Cao, D.; Zhu, X.; Zhao, Y. The Key Role of Reaction Temperature on a Polyol Synthesis of Water-Dispersible Iron Oxide Nanoparticles. *J. Magn. Magn. Mater.* **2021**, *540*, 168481. [CrossRef]
72. Abbasi, A.; Khojasteh, H.; Keihan, A.H.; Adib, K.; Sobhani-Nasab, A.; Rahimi-Nasrabadi, M. Co-Precipitation Synthesis of Ag-Doped $NiCr_2O_4$ Nanoparticles: Investigation of Structural, Optical, Magnetic, and Photocatalytic Properties. *J. Mater. Sci. Mater. Electron.* **2021**, *32*, 1413–1426. [CrossRef]
73. Adibi, M.; Mirkazemi, S.M.; Alamolhoda, S. The Influence of Citric Acid on the Microstructure and Magnetic Properties of Cobalt Ferrite Nanoparticles Synthesized by Hydrothermal Method. *Appl. Phys. A* **2021**, *127*, 497. [CrossRef]
74. Ansari, S.; Ficiarà, E.; Ruffinatti, F.; Stura, I.; Argenziano, M.; Abollino, O.; Cavalli, R.; Guiot, C.; D'Agata, F. Magnetic Iron Oxide Nanoparticles: Synthesis, Characterization and Functionalization for Biomedical Applications in the Central Nervous System. *Materials* **2019**, *12*, 465. [CrossRef]
75. Sun, J.; Jiang, K.; Wang, Y.; Liu, Y.; Wang, T.; Ding, S.; Zhang, X.; Xiong, W.; Zheng, F.; Yang, H.; et al. One-Pot Synthesis of Tumor-Microenvironment Responsive Degradable Nanoflower-Medicine for Multimodal Cancer Therapy with Reinvigorating Antitumor Immunity. *Adv. Health Mater.* **2023**, *12*, e2302016. [CrossRef]
76. Yan, Y.; Li, Y.; You, J.; Shen, K.; Chen, W.; Li, L. Morphology-Dependent Magnetic Hyperthermia Characteristics of Fe_3O_4 Nanoparticles. *Mater. Chem. Phys.* **2025**, *329*, 130045. [CrossRef]
77. Shen, K.; Li, L.; Tan, F.; Wu, S.; Jin, T.; You, J.; Chee, M.Y.; Yan, Y.; Lew, W.S. Hollow Spherical $Mn_{0.5}Zn_{0.5}Fe_2O_4$ Nanoparticles with a Magnetic Vortex Configuration for Enhanced Magnetic Hyperthermia Efficacy. *Nanoscale* **2023**, *15*, 17946–17955. [CrossRef] [PubMed]
78. Xu, Y.; Zhang, Y.; Li, N.; Yang, S.; Chen, J.; Hou, J.; Hou, C.; Huo, D. An Ultrasensitive Ratiometric Electrochemical Aptasensor Based on Metal-Organic Frameworks and Nanoflower-like Bi2CuO4 for Human Epidermal Growth Factor Receptor 2 Detection. *Bioelectrochemistry* **2023**, *154*, 108542. [CrossRef] [PubMed]
79. Ramamoorthy, S.; Reji, R.P.; Jayaraman, S.V.; Sundaramurthy, A. Fabrication of BiCuOS Nanoflowers Acting as Nanoarrays on Photonic Nanoparticles for Chemo-Photothermal Therapy. *Appl. Surf. Sci.* **2023**, *640*, 158360. [CrossRef]
80. Patel, H.; Parekh, K.; Fernel Gamarra, L.; Bustamante Mamani, J.; da Hora Alves, A.; Figueiredo Neto, A.M. In Vitro Evaluation of Magnetic Fluid Hyperthermia Therapy on Breast Cancer Cells Using Monodispersed $Mn_{0.5}Zn_{0.5}Fe_2O_4$ Nanoflowers. *J. Magn. Magn. Mater.* **2023**, *587*, 171275. [CrossRef]
81. Alizadeh, N.; Salimi, A.; Sham, T.-K.; Bazylewski, P.; Fanchini, G.; Fathi, F.; Soleimani, F. Hierarchical $Co(OH)_2/FeOOH/WO_3$ Ternary Nanoflowers as a Dual-Function Enzyme with pH-Switchable Peroxidase and Catalase Mimic Activities for Cancer Cell Detection and Enhanced Photodynamic Therapy. *Chem. Eng. J.* **2021**, *417*, 129134. [CrossRef]
82. García-Soriano, D.; Milán-Rois, P.; Lafuente-Gómez, N.; Rodríguez-Díaz, C.; Navío, C.; Somoza, Á.; Salas, G. Multicore Iron Oxide Nanoparticles for Magnetic Hyperthermia and Combination Therapy against Cancer Cells. *J. Colloid Interface Sci.* **2024**, *670*, 73–85. [CrossRef]
83. Theodosiou, M.; Sakellis, E.; Boukos, N.; Kusigerski, V.; Kalska-Szostko, B.; Efthimiadou, E. Iron Oxide Nanoflowers Encapsulated in Thermosensitive Fluorescent Liposomes for Hyperthermia Treatment of Lung Adenocarcinoma. *Sci. Rep.* **2022**, *12*, 8697. [CrossRef]
84. Fathy, M.; Hassan, H.; Hafez, H.; Soliman, M.; Abulfotuh, F.; Kashyout, A.E.H.B. Simple and Fast Microwave-Assisted Synthesis Methods of Nanocrystalline TiO_2 and rGO Materials for Low-Cost Metal-Free DSSC Applications. *ACS Omega* **2022**, *7*, 16757–16765. [CrossRef]
85. Shaw, S.K.; Kailashiya, J.; Gangwar, A.; Alla, S.K.; Gupta, S.K.; Prajapat, C.L.; Meena, S.S.; Dash, D.; Maiti, P.; Prasad, N.K. γ-Fe2O3 Nanoflowers as Efficient Magnetic Hyperthermia and Photothermal Agent. *Appl. Surf. Sci.* **2021**, *560*, 150025. [CrossRef]
86. Khorsand Zak, A.; Majid, W.H.A.; Wang, H.Z.; Yousefi, R.; Moradi Golsheikh, A.; Ren, Z.F. Sonochemical Synthesis of Hierarchical ZnO Nanostructures. *Ultrason. Sonochem.* **2013**, *20*, 395–400. [CrossRef]

87. Al-Qirby, L.M.; Radiman, S.; Siong, C.W.; Ali, A.M. Sonochemical Synthesis and Characterization of Co_3O_4 Nanocrystals in the Presence of the Ionic Liquid [EMIM][BF4]. *Ultrason. Sonochem.* **2017**, *38*, 640–651. [CrossRef]
88. Qi, C.; Zhu, Y.-J.; Wu, C.-T.; Sun, T.-W.; Jiang, Y.-Y.; Zhang, Y.-G.; Wu, J.; Chen, F. Sonochemical Synthesis of Hydroxyapatite Nanoflowers Using Creatine Phosphate Disodium Salt as an Organic Phosphorus Source and Their Application in Protein Adsorption. *RSC Adv.* **2016**, *6*, 9686–9692. [CrossRef]
89. Gulmez, C.; Altinkaynak, C.; Ozturkler, M.; Ozdemir, N.; Atakisi, O. Evaluating the Activity and Stability of Sonochemically Produced Hemoglobin-Copper Hybrid Nanoflowers against Some Metallic Ions, Organic Solvents, and Inhibitors. *J. Biosci. Bioeng.* **2021**, *132*, 327–336. [CrossRef]
90. Jafari-Nodoushan, H.; Mojtabavi, S.; Faramarzi, M.A.; Samadi, N. Organic-Inorganic Hybrid Nanoflowers: The Known, the Unknown, and the Future. *Adv. Colloid Interface Sci.* **2022**, *309*, 102780. [CrossRef]
91. Tran, T.D.; Nguyen, P.T.; Le, T.N.; Kim, M.I. DNA-Copper Hybrid Nanoflowers as Efficient Laccase Mimics for Colorimetric Detection of Phenolic Compounds in Paper Microfluidic Devices. *Biosens. Bioelectron.* **2021**, *182*, 113187. [CrossRef]
92. Liu, Y.; Zhu, X.; Lu, Y.; Wang, X.; Zhang, C.; Sun, H.; Ma, G. Antigen-Inorganic Hybrid Flowers-Based Vaccines with Enhanced Room Temperature Stability and Effective Anticancer Immunity. *Adv. Health Mater.* **2019**, *8*, e1900660. [CrossRef]
93. Dube, S.; Rawtani, D. Understanding Intricacies of Bioinspired Organic-Inorganic Hybrid Nanoflowers: A Quest to Achieve Enhanced Biomolecules Immobilization for Biocatalytic, Biosensing and Bioremediation Applications. *Adv. Colloid Interface Sci.* **2021**, *295*, 102484. [CrossRef]
94. Bilal, M.; Anh Nguyen, T.; Iqbal, H.M.N. Multifunctional Carbon Nanotubes and Their Derived Nano-Constructs for Enzyme Immobilization—A Paradigm Shift in Biocatalyst Design. *Coord. Chem. Rev.* **2020**, *422*, 213475. [CrossRef]
95. Lei, Z.; Gao, C.; Chen, L.; He, Y.; Ma, W.; Lin, Z. Recent Advances in Biomolecule Immobilization Based on Self-Assembly: Organic–Inorganic Hybrid Nanoflowers and Metal–Organic Frameworks as Novel Substrates. *J. Mater. Chem. B* **2018**, *6*, 1581–1594. [CrossRef]
96. Aydemir, D.; Gecili, F.; Özdemir, N.; Nuray Ulusu, N. Synthesis and Characterization of a Triple Enzyme-Inorganic Hybrid Nanoflower (TrpE@ihNF) as a Combination of Three Pancreatic Digestive Enzymes Amylase, Protease and Lipase. *J. Biosci. Bioeng.* **2020**, *129*, 679–686. [CrossRef]
97. He, H.; Fu, C.; An, Y.; Feng, J.; Xiao, J. Biofunctional Hollow γ-MnO_2 Microspheres by a One-Pot Collagen-Templated Biomineralization Route and Their Applications in Lithium Batteries. *RSC Adv.* **2021**, *11*, 37040–37048. [CrossRef]
98. Subramani, I.G.; Perumal, V.; Gopinath, S.C.B.; Mohamed, N.M.; Ovinis, M.; Sze, L.L. 1,1′-Carbonyldiimidazole-Copper Nanoflower Enhanced Collapsible Laser Scribed Graphene Engraved Microgap Capacitive Aptasensor for the Detection of Milk Allergen. *Sci. Rep.* **2021**, *11*, 20825. [CrossRef]
99. Makarov, V.V.; Love, A.J.; Sinitsyna, O.V.; Makarova, S.S.; Yaminsky, I.V.; Taliansky, M.E.; Kalinina, N.O. "Green" Nanotechnologies: Synthesis of Metal Nanoparticles Using Plants. *Acta Nat.* **2014**, *6*, 35–44. [CrossRef]
100. Molina, G.A.; Esparza, R.; López-Miranda, J.L.; Hernández-Martínez, A.R.; España-Sánchez, B.L.; Elizalde-Peña, E.A.; Estevez, M. Green Synthesis of Ag Nanoflowers Using Kalanchoe Daigremontiana Extract for Enhanced Photocatalytic and Antibacterial Activities. *Colloids Surf. B Biointerfaces* **2019**, *180*, 141–149. [CrossRef]
101. Somturk Yilmaz, B. Anticancer and Antimicrobial Activities of Quercetin-CuhNFs and Quercetin-CohNFs on MDA-MB-231 (Breast Cancer). *J. Inorg. Organomet. Polym.* **2024**, *34*. [CrossRef]
102. Yilmaz, B.S.; Bekci, H.; Altiparmak, A.; Uysal, S.; Şenkardeş, İ.; Zengin, G. Determination of Anticancer Activity and Biosynthesis of Cu, Zn, and Co Hybrid Nanoflowers with *Tribulus terrestris* L. Extract. *Process Biochem.* **2024**, *138*, 14–22. [CrossRef]
103. Gao, J.; Liu, H.; Tong, C.; Pang, L.; Feng, Y.; Zuo, M.; Wei, Z.; Li, J. Hemoglobin-$Mn_3(PO_4)_2$ Hybrid Nanoflower with Opulent Electroactive Centers for High-Performance Hydrogen Peroxide Electrochemical Biosensor. *Sens. Actuators B Chem.* **2020**, *307*, 127628. [CrossRef]
104. Hao, M.; Fan, G.; Zhang, Y.; Xin, Y.; Zhang, L. Preparation and Characterization of Copper-Brevibacterium Cholesterol Oxidase Hybrid Nanoflowers. *Int. J. Biol. Macromol.* **2019**, *126*, 539–548. [CrossRef]
105. Chen, J.; Guo, Z.; Xin, Y.; Gu, Z.; Zhang, L.; Guo, X. Organic–Inorganic Hybrid Nanoflowers: A Comprehensive Review of Current Trends, Advances, and Future Perspectives. *Coord. Chem. Rev.* **2023**, *489*, 215191. [CrossRef]
106. Xiang, J.Y.; Tu, J.P.; Zhang, L.; Zhou, Y.; Wang, X.L.; Shi, S.J. Self-Assembled Synthesis of Hierarchical Nanostructured CuO with Various Morphologies and Their Application as Anodes for Lithium Ion Batteries. *J. Power Sources* **2010**, *195*, 313–319. [CrossRef]
107. Zhang, M.; Zhang, Y.; Yang, C.; Ma, C.; Tang, J. Enzyme-Inorganic Hybrid Nanoflowers: Classification, Synthesis, Functionalization and Potential Applications. *Chem. Eng. J.* **2021**, *415*, 129075. [CrossRef]
108. Yin, N.Q.; Wu, P.; Yang, T.H.; Wang, M. Preparation and Study of a Mesoporous Silica-Coated Fe_3O_4 Photothermal Nanoprobe. *RSC Adv.* **2017**, *7*, 9123–9129. [CrossRef]
109. Espinosa, A.; Bugnet, M.; Radtke, G.; Neveu, S.; Botton, G.A.; Wilhelm, C.; Abou-Hassan, A. Can Magneto-Plasmonic Nanohybrids Efficiently Combine Photothermia with Magnetic Hyperthermia? *Nanoscale* **2015**, *7*, 18872–18877. [CrossRef] [PubMed]
110. Liu, X.L.; Ng, C.T.; Chandrasekharan, P.; Yang, H.T.; Zhao, L.Y.; Peng, E.; Lv, Y.B.; Xiao, W.; Fang, J.; Yi, J.B.; et al. Synthesis of Ferromagnetic $Fe_{0.6}Mn_{0.4}O$ Nanoflowers as a New Class of Magnetic Theranostic Platform for In Vivo T1-T2 Dual-Mode Magnetic Resonance Imaging and Magnetic Hyperthermia Therapy. *Adv. Healthc. Mater.* **2016**, *5*, 2092–2104. [CrossRef]

111. Saeed, M.; Iqbal, M.Z.; Ren, W.; Xia, Y.; Liu, C.; Khan, W.S.; Wu, A. Controllable Synthesis of Fe_3O_4 Nanoflowers: Enhanced Imaging Guided Cancer Therapy and Comparison of Photothermal Efficiency with Black-TiO_2. *J. Mater. Chem. B* **2018**, *6*, 3800–3810. [CrossRef]
112. Huang, J.; Guo, M.; Ke, H.; Zong, C.; Ren, B.; Liu, G.; Shen, H.; Ma, Y.; Wang, X.; Zhang, H.; et al. Rational Design and Synthesis of γFe2O3@Au Magnetic Gold Nanoflowers for Efficient Cancer Theranostics. *Adv. Mater.* **2015**, *27*, 5049–5056. [CrossRef]
113. Benassai, E.; Hortelao, A.C.; Aygun, E.; Alpman, A.; Wilhelm, C.; Saritas, E.U.; Abou-Hassan, A. High-Throughput Large Scale Microfluidic Assembly of Iron Oxide nanoflowers@PS-b-PAA Polymeric Micelles as Multimodal Nanoplatforms for Photothermia and Magnetic Imaging. *Nanoscale Adv.* **2023**, *6*, 126–135. [CrossRef]
114. Nicolás-Boluda, A.; Vaquero, J.; Laurent, G.; Renault, G.; Bazzi, R.; Donnadieu, E.; Roux, S.; Fouassier, L.; Gazeau, F. Photothermal Depletion of Cancer-Associated Fibroblasts Normalizes Tumor Stiffness in Desmoplastic Cholangiocarcinoma. *ACS Nano* **2020**, *14*, 5738–5753. [CrossRef]
115. Curcio, A.; Silva, A.K.A.; Cabana, S.; Espinosa, A.; Baptiste, B.; Menguy, N.; Wilhelm, C.; Abou-Hassan, A. Iron Oxide Nanoflowers @ CuS Hybrids for Cancer Tri-Therapy: Interplay of Photothermal Therapy, Magnetic Hyperthermia and Photodynamic Therapy. *Theranostics* **2019**, *9*, 1288–1302. [CrossRef]
116. Jing, X.; Xu, Y.; Liu, D.; Wu, Y.; Zhou, N.; Wang, D.; Yan, K.; Meng, L. Intelligent Nanoflowers: A Full Tumor Microenvironment-Responsive Multimodal Cancer Theranostic Nanoplatform. *Nanoscale* **2019**, *11*, 15508–15518. [CrossRef] [PubMed]
117. Chen, W.; Wang, X.; Zhao, B.; Zhang, R.; Xie, Z.; He, Y.; Chen, A.; Xie, X.; Yao, K.; Zhong, M.; et al. CuS–MnS2 Nano-Flowers for Magnetic Resonance Imaging Guided Photothermal/Photodynamic Therapy of Ovarian Cancer through Necroptosis. *Nanoscale* **2019**, *11*, 12983–12989. [CrossRef]
118. Neelgund, G.M.; Oki, A.; Bandara, S.; Carson, L. Photothermal Effect and Cytotoxicity of CuS Nanoflowers Deposited over Folic Acid Conjugated Nanographene Oxide. *J. Mater. Chem. B* **2021**, *9*, 1792–1803. [CrossRef] [PubMed]
119. Liao, X.; Zheng, Y.; Lin, Z.; Shen, Y.; Lin, H.; Liu, X.; Zhang, D.; Li, B. Self-Assembled Metallo-Supramolecular Nanoflowers for NIR/Acidic-Triggered Multidrug Release, Long-Term Tumor Retention and NIR-II Fluorescence Imaging-Guided Photo-Chemotherapy. *Chem. Eng. J.* **2020**, *400*, 125882. [CrossRef]
120. Wu, M.; He, S.; Hu, X.; Chen, J.; Ha, E.; Ai, F.; Ji, T.; Hu, J.; Ruan, S. A Near-Infrared Light Triggered Composite Nanoplatform for Synergetic Therapy and Multimodal Tumor Imaging. *Front. Chem.* **2021**, *9*, 695511. [CrossRef] [PubMed]
121. Zhang, X.; Jin, L.-H.; Li, Y.-Y.; Xiao, Z.-Z.; Feng, Y.; Lin, Y.-W.; Zhang, Y. Portable Self-Powered Photoelectrochemical Immunosensor Based on Cu_3 SnS_4 Nanoflower for Ultra-Sensitive and Real-Time Detection of Human Cytochrome *c*. *Inorg. Chem. Front.* **2023**, *10*, 5591–5601. [CrossRef]
122. Somtürk Yilmaz, B. Antimicrobial and Anticancer Activity of Gallic Acid–Cu(II) Hybrid Nanoflowers and Gallic Acid–Zn(II) Hybrid Nanoflowers. *J. Inorg. Organomet. Polym.* **2024**. [CrossRef]
123. Zhang, H.; Chen, Y.; Cai, Y.; Liu, J.; Liu, P.; Li, Z.; An, T.; Yang, X.; Liang, C. Paramagnetic CuS Hollow Nanoflowers for T2-FLAIR Magnetic Resonance Imaging-Guided Thermochemotherapy of Cancer. *Biomater. Sci.* **2019**, *7*, 409–418. [CrossRef]
124. Eskikaya, O.; Özdemir, S.; Gonca, S.; Dizge, N.; Balakrishnan, D.; Shaik, F.; Senthilkumar, N. A Comparative Study of Iron Nanoflower and Nanocube in Terms of Antibacterial Properties. *Appl. Nanosci.* **2023**, *13*, 5421–5433. [CrossRef]
125. Ingle, A.P.; Rai, M. Copper Nanoflowers as Effective Antifungal Agents for Plant Pathogenic Fungi. *IET Nanobiotechnol.* **2017**, *11*, 546–551. [CrossRef]
126. Gkika, D.A.; Magafas, L.; Cool, P.; Braet, J. Balancing Nanotoxicity and Returns in Health Applications: The Prisoner's Dilemma. *Toxicology* **2018**, *393*, 83–89. [CrossRef] [PubMed]
127. Gkika, D.A.; Vordos, N.; Magafas, L.; Mitropoulos, A.C.; Kyzas, G.Z. Risk Return Profile of Nanomaterials. *J. Mol. Struct.* **2021**, *1228*, 129740. [CrossRef]
128. Talev, J.; Kanwar, J.R. Iron Oxide Nanoparticles as Imaging and Therapeutic Agents for Atherosclerosis. *Semin. Thromb. Hemost.* **2020**, *46*, 553–562. [CrossRef] [PubMed]

Disclaimer/Publisher's Note: The statements, opinions and data contained in all publications are solely those of the individual author(s) and contributor(s) and not of MDPI and/or the editor(s). MDPI and/or the editor(s) disclaim responsibility for any injury to people or property resulting from any ideas, methods, instructions or products referred to in the content.